U.PORTO

Mestrado

Toxicologia Analítica Clínica e Forense

Metabolomic studies for the toxicity evaluation of nanoparticles used for biomedical purposes.

Mariana Machado Pereira

M

2020

Mariana Machado Pereira

Metabolomic studies for the toxicity evaluation of nanoparticles used for biomedical purposes.

Dissertação do 2º Ciclo de Estudos Conducente ao Grau de Mestre em Toxicologia Analítica Clínica e Forense

Trabalho realizado sob a orientação de:

Professora Doutora Helena Carmo, Professora Auxiliar, Departamento Ciências Biológicas, Laboratório de Toxicologia, Faculdade de Farmácia da Universidade do Porto

Professora Doutora Maria de Lourdes P. A. S. Bastos, Professora Catedrática, Departamento Ciências Biológicas, Laboratório de Toxicologia, Faculdade de Farmácia da Universidade do Porto

Outubro 2020

Declarações

De acordo com a legislação em vigor, não é permitida a reprodução de qualquer parte desta dissertação/tese

Agradecimentos

Queria, antes de mais, expressar o meu agradecimento a toda a gente que tornou isto possível.

Primeiramente, queria agradecer à minha orientadora, Dr[a]. Helena Carmo, por me ter dado esta oportunidade e por toda a ajuda e apoio que me deu na minha jornada, estando sempre presente para qualquer dúvida ou problema que eu tive. Também queria agradecer por me ter apresentado a este tema, o qual tive muito interesse e gosto em descobrir mais. Do mesmo modo, quero agradecer à minha co-orientadora, Dr[a]. Maria de Lurdes Bastos, pela disponibilidade que teve para me ajudar com a correção desta dissertação.

À Dra. Diana Dias da Silva, queria agradecer toda a paciência que teve para mim, mesmo não sendo minha orientadora ajudou como se fosse, e não tenho palavras para expressar o quão agradecida estou. Ao Dr. Miguel Peixoto de Almeida e à Dr[a]. Eulália Pereira queria agradecer por generosamente terem fornecido as nanopartículas, este trabalho nunca teria sido possível se não fosse o caso. À Ana Rita Lima, obrigada pela ajuda na fase final da minha tese e pela paciência para as mil perguntas que tive. À Rita Roque, queria agradecer pela assistência nos isolamentos, nunca conseguiria ter acabado a tese sem essa ajuda.

Ao meu namorado, Rogério, queria agradecer por estes mais de três anos e meio, obrigada por aturares a minha constante divagação e por te manteres comigo apesar de tudo. Não conseguia imaginar como seria a minha vida sem ti, estes anos tinham sido muito menos interessantes.

Ao meu pessoal do secundário, obrigada por continuarem lá, não é todos os dias que se vê um grupo de pessoas ainda irem de férias juntas após tantos anos separados. Também não podia deixar de agradecer à Sofia, são dez anos de amizade apesar da distância, espero sejam muitos mais ainda.

Não posso não agradecer às minhas hienas, mais em específico a algumas. À Melo, a pessoa que está comigo desde o secundário, obrigada por me dares de comer e por todas as maratonas, ainda vêm muitas mais bro. À Bárbara, foi um prazer ter a relação amor ódio estes 5 anos, o mestrado tinha sido muito aborrecido sem ti lá para te achincalhar e para stressarmos juntas. À Tatiana, obrigada por todas as conversas e pela confiança, ter alguém com quem se pode falar de tudo sem problemas é raro. À Márcia e ao João, por serem as primeiras pessoas que me consideraram uma boa escolha para amizade na faculdade. Ao Vítor e ao Sérgio, pela nossa amizade, apesar de tudo. Por último, à Maria, Marcus, Rita, Lili e Xavier, obrigada por lidarem comigo e por terem decidido que afinal esta pessoa rude até daria uma boa amiga, espero que continuem a achar isso. Também tenho de agradecer à Rosa Melo, porque nunca esperei encontrar alguém fora do meu ano com a qual fosse ter

uma relação tão forte, que dura mesmo depois de ter saído da faculdade. Obrigada por estares lá sempre que eu preciso, não te fartes de mim porque eu não vou de ti.

Por último queria agradecer à minha família. À minha mãe e ao meu pai, que sempre me incentivaram a ir atrás do que eu quero e me apoiaram em todas as decisões inquestionavelmente. Ao meu irmão, que é um bocado insuportável, mas que quando eu preciso está lá para me fazer esquecer dos meus problemas. À Alexandra e ao Eduardo, mais irmãos que primos, e que mesmo sendo mais novos conseguem ser a voz da razão às vezes. Aos meus avós, papis, à minha madrinha e ao Luís, obrigada por estarem lá quando eu preciso de desabafar e para me acalmarem com comida e mimo, não podia pedir melhor.

A todos, queria deixar o meu maior agradecimento, nunca poderia ter chegado aonde cheguei sem a vossa ajuda e apoio incondicional.

ABSTRACT

Nanomaterials (NMs) are compounds that have been emerging in many fields, mainly in nanomedicine. With this, their biosafety to humans and other organisms must be characterized. In this study, primary rat hepatocytes were exposed to low concentrations (nM range) of six different NMs, namely gold nanospheres of three sizes (12, 40, and 60 nm, 1.50, 0.017, and 7.5×10^{-4} nM), gold nanostars (60 nm, 0.017 nM), silver nanostars (200 nm, 0.010 nM) and selenium nanospheres (300 nm, 1.67×10^{-3} nM), and their cytotoxicity and metabolic changes were determined. For this, the MTT and NR assays were used to obtain the highest non-cytotoxic concentration of each NM, which was then used for metabolomics, performed through GC-MS. The results of the cytotoxicity assays showed that all NMs, but the selenium nanospheres, exhibited no decrease in cell viability at the concentrations tested. Several other concentrations of selenium nanospheres were tested to determine the maximum non-cytotoxic concentration, which was 1.67×10^{-3} nM.

Regarding the metabolomic results, several metabolites and pathways were observed to be altered between the control and exposed cells for all NMs. Generally, most metabolites were downregulated. All the gold NMs presented dysregulation in fatty acid/lipid, energy and protein metabolism as well as oxidative stress, with a particular effect in the propanoate metabolism pathway. The smaller (12 and 40 nm) gold nanospheres caused alteration in carbohydrate metabolism, while the larger (60 nm) seemed to have caused inflammation. Gold nanostars provoked upregulation of L-alanine (one of the few metabolites that were upregulated). The selenium nanospheres were associated with interferences in energy and protein metabolism, amino acid synthesis, and changes in cell structure and processes, like cell differentiation, growth, and apoptosis. Lastly, the silver nanostars changed the protein, lipid, and nucleic acid metabolism, with indications of oxidative stress and cell cycle arrest. With these results, we concluded that NMs can present effects in several metabolic pathways, with overlapping effects across most of them, like dysregulations in protein, lipid, and energy metabolism. These alterations were detected at non-cytotoxic concentrations, which proves that NMs can influence cells even at very low concentrations and that highly sensitive methods, like metabolomics, are of utmost relevance in nanotoxicity since classical *in vitro* assays are not indicative of all the early effects that NMs can cause.

Keywords: cytotoxicity, hepatotoxicity, metabolomics, nanomaterials

RESUMO

A aplicação de nanomateriais (NMs) tem surgido em diversos campos, principalmente na nanomedicina. Por isso, a sua segurança em humanos e outros organismos deve ser caracterizada. Neste estudo, hepatócitos primários de rato foram expostos a baixas concentrações (nM) de seis NMs diferentes, nomeadamente nanoesferas de ouro de três tamanhos distintos (12, 40 e 60 nm 1.50, 0.017 e 7.5×10^{-4} nM), nanoestrelas de ouro (60 nm, 0.017 nM), nanoestrelas de prata (200 nm, 0.010 nM) e nanoesferas de selénio (300 nm, 1.67×10^{-3} nM), e sua citotoxicidade e alterações metabólicas foram determinadas. Para isso, os ensaios de MTT e NR foram utilizados para identificar a maior concentração não citotóxica de cada NM, que foi então utilizada para a metabolómica, realizada por CG-MS. Os resultados dos ensaios de citotoxicidade mostraram que todos os NMs, exceto as nanoesferas de selénio, não produziram diminuição na viabilidade celular nas concentrações testadas. Várias outras concentrações de nanoesferas de selénio foram testadas para determinar a concentração máxima não citotóxica, que foi de $1{,}67 \times 10^{-3}$ nM. Em relação aos resultados da metabolómica, vários metabolitos e vias apareceram alterados nas células expostas a todos os NMs, comparativamente às células controlo. Em geral, os níveis da maioria dos metabolitos diminuíram. Todos os NMs de ouro causaram desregulação no metabolismo de ácidos gordos/lípidos, energia e proteínas, bem como stresse oxidativo, com efeito particular na via de metabolismo do propanoato. As nanoesferas de ouro mais pequenas (12 e 40 nm) apresentaram alteração no metabolismo de carboidratos, enquanto as maiores (60 nm) apresentaram possível inflamação após a exposição. As nanoestrelas de ouro originaram o aumento da L-alanina, um dos poucos metabolitos que foram regulados positivamente. As nanoesferas de selénio foram associadas a interferências no metabolismo energético e proteico, síntese de aminoácidos e mudanças na estrutura e processos celulares, como diferenciação, crescimento e apoptose. Por fim, as nanoestrelas de prata mudaram o metabolismo de proteínas, lipídios e ácidos nucleicos, com indicações de stresse oxidativo e bloqueio do ciclo celular.

Com estes resultados concluímos que os NMs podem apresentar efeitos em diversas vias metabólicas, com várias sendo alteradas pela maioria dos NMs testados, como desregulações no metabolismo proteico, lipídico e energético. Essas alterações foram detetadas para concentrações não citotóxicas, o que prova que os NMs podem influenciar células mesmo em concentrações muito baixas e que métodos altamente sensíveis, como a metabolómica, são de extrema relevância no estudo da nanotoxicidade, uma vez que os ensaios clássicos *in vitro* não fornecem indicação precoce de todos os efeitos que os NMs podem causar.

Palavras-chave: citotoxicidade, hepatotoxicidade, metabolómica nanomateriais

TABLE OF CONTENTS

1. Introduction 1
1.1 Medical applications of NMs 2
1.1.1 Diagnostics 2
1.1.2 Therapy 3
1.2 Biokinetics of NMs 4
1.2.1 Absorption 4
1.2.2 Distribution 5
1.2.3 Metabolism 5
1.2.4 Excretion 6
1.3 Factors that affect the biokinetics of NMs 7
1.3.1 Hydrophobicity and hydrophilicity of the surface 7
1.3.2 Surface charge 7
1.3.3 Size 8
1.4 Mechanisms of toxicity of NMs 8
1.4.1 Oxidative stress and mitochondrial damage 9
1.4.2 Inflammatory effect 9
1.4.3 Genotoxicity 10
1.5 Metabolomics 11
1.5.1 Analytical platforms 12
1.5.2 Untargeted versus targeted metabolomics 12
1.5.3 Fingerprinting versus footprinting 13
1.5.4 Metabolomics in nanotoxicology 13
1.6 Nanoparticles 15
1.6.1 Gold nanoparticles 15
1.6.2 Selenium nanoparticles 16
1.6.3 Silver nanoparticles 17
2. Objectives 19
3. Materials and methods 20

3.1 Chemicals and reagents 20
3.2 Synthesis and characterization of NPs 20
3.3 Animals 23
3.4 Isolation of primary hepatocytes 23
3.5 Cell plating and exposure 25
3.6 Cytotoxic assays 26
3.7 Metabolomics 26
3.7.1 Collection of Samples 26
3.7.2 Derivatization of analytes 27
3.7.3 GC-MS analysis 27
3.7.4 GC-MS data pre-processing 28
3.8 Statistical analysis 28
4. Results 30
4.1 Characterization of nanoparticles 30
4.2 Cytotoxicity 32
4.3 Metabolomics results 33
5. Discussion 45
6. Conclusion 51
7. Future perspectives 51
8. References 52

FIGURES INDEX

Figure 1 – Scaffolding created using nanomaterials for cell fixation with functional components for tissue engineering. The functional components can be growth factors or compounds that alter the properties of NMs (like charge). 3
Figure 2 – Metabolism of NMs. 6
Figure 3 – Biokinetic components altered by nanomaterials characteristics. 8
Figure 4 – Mechanisms of toxicity of NMs. 11
Figure 5 – Nanoparticles. From left to right: selenium nanoparticles, 60 nm gold nanoparticles, 40 nm gold nanoparticles, 12 nm gold nanoparticles, gold nanostars and silver nanostars. 22
Figure 6 – Hepatocyte isolation set up. Thermostatic water bath (left), peristaltic pump (center)..... 24
Figure 7 – UV-Vis spectrum of the nanoparticles and maximum extinction wavelength. ..31
Figure 8 – TEM images of nanoparticles. SeNPs (A, B), AgNSs (C, D), AuNPs (E) and AuNSs (F). C, D, E and F are representative. All images were provided by the investigators of the LAQV/REQUIMTE Laboratory, Department of Chemistry and Biochemistry, Faculty of Sciences, University of Porto. 31
Figure 9 – Percentage of MTT reduction (left) and percentage of NR incorporation (right) for 12 nm AuNPs (1.50 nM), 40 nm AuNPs (0.017 nM), 60 nm AuNPs (7.5×10^{-4} nM), AuNSs (0.017 nM) and AgNSs (0.010 nM). Comparison with controls performed with one-way ANOVA Kruskal-Wallis test. *p ≤ 0.05. 32
Figure 10 – Percentage of MTT reduction (left) and percentage of NR incorporation (right) for SeNPs. Concentrations: 10x (0.010 nM), 20x (5.0×10^{-3} nM), 30x (3.33×10^{-3} nM), 40x (2.5×10^{-3} nM), 50x (2.0×10^{-3} nM), 60x (1.67×10^{-3} nM), 70x (1.43×10^{-3} nM), 80x (1.25×10^{-3} nM) and 90x (1.11×10^{-3} nM). Comparison with controls performed with one-way ANOVA Kruskal-Wallis test. *p ≤ 0.05, **p ≤ 0.01, ***p ≤ 0.001 and ****p ≤ 0.0001..... 32
Figure 11 – PCA of QCs (green) and samples (light blue). The QCs represent a pool of all samples, controls and treatments, and are identical, which should lead to equal samples. Since they are all together, the reproducibility was confirmed. 33
Figure 12 – PLS-DA models. A – Control (green) *vs*. 24 h exposure to 1.67×10^{-3} nM SeNPs (red); B – control (green) *vs*. 24 h exposure to 1.50 nM 12 nm AuNPs (light blue); C – control (green) *vs*. 24 h exposure to 0.017 nM 40 nm AuNPs (yellow); D – control (green) *vs*. 24 h exposure to 0.017 nM AuNSs (purple); F – control (green) *vs*. 24 h exposure to 0.010 nM AgNSs (dark blue). Q2 superior to 0.5 indicates a discrimination between control and NP exposure samples. 34

Figure 13 – Validation of PLS-DA models through permutation tests (200 permutations, two components). A – 24 h exposure to 1.67×10^{-3} nM SeNPs; B – 24 h exposure to 1.50 nM 12 nm AuNPs; C – 24 h exposure to 0.017 nM 40 nm AuNPs; D – 24 h exposure to 7.5×10^{-4} nM 60 nm AuNPs; E – 24 h exposure to 0.017 nM AuNSs; F - 24 h exposure to 0.010 nM AgNSs. Validation required Q2 (blue) and R2 (green) values lower than original (far right) and intersection of regression line of Q2 values (blue) with x-axis at or below zero. 35
Figure 14 – Boxplots of altered metabolites after 24 h exposure of cells to 1.67×10^{-3} nM of SeNPs. * $p<0.05$. 40
Figure 15 – Boxplots of altered metabolites after 24 h exposure of cells to 1.50 nM of 12 nm AuNPs. * $p<0.05$, ** $p<0.01$. 40
Figure 16 – Boxplots of altered metabolites after 24 h exposure of cells to 0. 017 nM of 40 nm AuNPs. * $p< 0.05$, ** $p<0.01$. 40
Figure 17 – Boxplots of altered metabolites after 24 h exposure of cells to 7.5×10^{-4} of 60 nm AuNPs. * $p<0.05$, ** $p<0.01$. 40
Figure 18 – Boxplots of altered metabolites after 24 h exposure of cells to 0.017 nM of AuNSs. * $p<0.05$, ** $p<0.01$. 41
Figure 19 – Boxplots of altered metabolites after 24 h exposure of cells to 0.010 nM of AgNSs. * $p<0.05$. 41
Figure 20 – Metabolic pathways significantly altered in cells exposed to 1.67×10-3 nM of SeNPs for 24 h. A- aminoacyl-tRNA biosynthesis (L-aspartic acid, L-serine. p=0.002763); B- Arginine biosynthesis (L-aspartic acid, p= 0.02687); C- Nicotinate and nicotinamide metabolism (L-aspartic acid, p= 0.028771); D- Histidine metabolism (L-aspartic acid, p= 0.030669); E- Pantothenate and CoA biosynthesis (L-aspartic acid, p= 0.036348); F- beta-Alanine metabolism (L-aspartic acid, p= 0.040123); G- Sphingolipid metabolism (L-serine, p= 0.040123); H -Galactose metabolism (D-galactose, p= 0.051386); I- Alanine, aspartate and glutamate metabolism (L-aspartic acid, p= 0.053254). 42
Figure 21 – Metabolic pathways significantly altered in cells exposed to 7.5×10^{-4} nM of 60 nm AuNPs for 24 h. A- Propanoate metabolism (2-hydroxybutyric acid, p=0.043887).... 42
Figure 22 – Metabolic pathways significantly altered in cells exposed to 0.017 nM of AuNSs for 24 h. A- Selenocompound metabolism (L-alanine, p=0.038237); B- Propanoate metabolism (2-hydroxybutyric acid, p=0.043887); C- Alanine, aspartate and glutamate metabolism (L-alanine, p=0.053254). 43
Figure 23 – Metabolic pathways significantly altered in cells exposed to 0.010 nM of AgNSs for 24 h. A- D-Glutamine and D-glutamate metabolism (L-glutamine, p= 0.011575); B- Nitrogen metabolism (L-glutamine, p=0.011575); C- Arginine biosynthesis (L-glutamine, p=0.02687); D- Alanine, aspartate and glutamate metabolism (L-glutamine, p=0.053254). 43

TABLES INDEX

Table 1 – Characterization of the NPs. 30
Table 2 – List of discriminant metabolites for all NPs. 36
Table 3 – List of discriminant metabolites with p-value, percentage of variation and effect size. 38

LIST OF ABBREVIATIONS

λ_{max} – maximum extinction wavelengths

AgNPs – silver nanoparticles/nanospheres

AgNSs – silver nanostars

AuNPs – gold nanoparticles/nanospheres

AuNSs – gold nanostars

Cit – citrate

DLS – dynamic light scattering

EGTA – ethylene glycol-bis(2-aminoethylether)-N,N,N′,N′-tetraacetic acid

ELS – electrophoretic light scattering

GC – gas chromatography

GSH – reduced glutathione

GSSG – oxidized glutathione

HA – neutral hydroxylamine

HBSS – hanks balanced salt solution

HEPES - 4-(2-hydroxyethyl)-1-piperazineethanesulfonic acid

HepG2 – human caucasian hepatocyte carcinoma cells line

KH – Krebs-Henseleit buffer

LC – liquid chromatography

L-02 – normal human hepatocytes

MEM – minimum essential medium

MS – mass spectrometry

MS/MS – tandem mass spectrometry

MTT – 3-(4,5-dimethylthiazol-2-yl)-2,5-diphenyltetrazolium bromide

MUA – 11-mercaptoundecanoic acid

m/z – mass/charge ratio

NMR – nuclear magnetic resonance

NMs – nanomaterials

NPs – nanoparticles

NR – neutral red

NTA – nanoparticle tracking analysis

PCA – principal component analysis

PLS-DA – partial least squares discriminant analysis

PSSNa – poly-(sodiumsterene sulfonate)

PVP – poly-vinylpyrrolidone

QCs – quality controls

ROS – reactive oxygen species

RT – retention time

SeNPs – selenium nanoparticles/nanospheres

TCA – tricarboxylic acid cycle

TEM – transmission electron microscopy

UV-Vis – ultraviolet-visible spectroscopy

VIP – variable importance of projection

ZnO NPs – zinc oxide nanoparticles

1. INTRODUCTION

Nanotechnology allows the design, fabrication, and application of nanomaterials (NMs) and nanostructures, as well as the study of their physicochemical properties (also termed nanoscience) (Cao and Wang, 2011). The recommended definition of NM by the European Union is "a natural, incidental or manufactured material containing particles, in an unbound state or as an aggregate or as an agglomerate and where, for 50% or more of the particles in the number size distribution, one or more external dimensions is in the size range 1 nm - 100 nm" (http://ec.europa.eu/environment/chemicals/nanotech/faq/definition_en.htm). Some authors, however, define NMs as a material with external dimensions in the nanoscale, within a range between 1 nm – 1000 nm (Buzea and Pacheco, 2017). NMs can be classified according to their dimensional structures, that is, how many of the three external dimensions are in the nanoscale area. Accordingly, the NMs can be: zero-dimensional, when all three dimensions are in the nanoscale, such as spheres and fullerenes; one-dimensional, when one of the three dimensions is beyond the nanoscale, like nanorods and nanotubes; two-dimensional, when only one of the dimensions is in the nanoscale, like nanowalls and nanofibers; and three-dimensional, when none of the dimensions are in the nanoscale but they present features at the nanoscale, such as carbon nanobuds, that have both nanotubes and fullerene films (Saleh and Gupta, 2016). Synthesis of NMs can be top-down or bottom-up. In the former, bulk materials are taken and reduced to build the NMs, which gives rise to many defects, such as surface imperfections. In the latter, the NM is built in an atom-by-atom approach, which gives more chemically homogenous NMs with fewer defects (Cao and Wang, 2011).

Due to the very small size of NMs, they exhibit physicochemical properties very different from their bulk counterparts. They have a very large surface area as well as surface to volume ratio, which makes the behavior of NMs controlled by their surface properties rather than by their volume. This will give NMs characteristics like unique optical and electrical properties, as well as greater hardness, strength, and abrasion resistance. The larger surface area, coupled with the presence of more angles, edges, and crystal defects, give NMs higher chemical reactivity. There is also a reduction of the melting temperature relative to the bulk materials, and changes in the magnetic properties, like superparamagnetism and magnetostriction (deformation of the NMs under a magnetic field) (Dolez, 2015).

NMs have been used in several sectors due to these unique properties. Applications can be found in the food sector, like in agriculture, animal feed and food processing, packaging, and storage (Peters *et al.*, 2016). NMs can also be found in electronics, energy storage and production, and automobile and space engineering (Bachhav and Deore, 2015). Uses in cosmetics are also common, like in the formulation of sunscreens (de Melo *et al.*,

2015), and nanomedicine, that encompasses the application of NMs in the pharmaceutical and medicinal fields, which has been of great interest over the last years. The development of methods for nano-delivery of drugs and for *in vitro* diagnostics have been the major areas of investment in nanomedicine (Valavanidis and Vlachogianni, 2016).

1.1 MEDICAL APPLICATIONS OF NMS

Nanomedicine is a field with increasing interest due to the new possibilities that NMs bring to medicine, mainly in diagnostics and in therapy.

1.1.1 DIAGNOSTICS

One of the major tools for diagnosis is the medical imaging of tissues and organs. To this end, contrast agents are needed to provide a contrast of what is being analyzed with the surroundings, and they should be specific to the location of interest (Fadeel *et al.*, 2013). NM-based contrast agents have some advantages in relation with traditional ones, namely: they stay in circulation for a longer period and have controlled biological clearance pathways, which provides more time to perform the analysis (Bayford *et al.*, 2017); their physicochemical properties (shape, size, surface) are tunable (Sakamoto *et al.*, 2010) and they allow for the functionalization of the surface of NMs with organic groups or polymers. This can modify their physicochemical characteristics to increase cellular uptake, for example, as it happens with the functionalization of silica nanoparticles (NPs) with polyethyleneimine (Atluri and Jensen, 2017). One example of NMs of great interest in imaging diagnostics are the superparamagnetic iron oxide nanoparticles used in magnetic resonance imaging since they have magnetic properties, are good enhancers of proton relaxation, and do not aggregate after the magnetic field ceases to be applied. After they serve their purpose, these NPs are phagocytized and metabolized into iron (soluble and non-superparamagnetic) that joins with the iron pools of the organism (Luque-Michel *et al.*, 2017).

Another type of diagnosis is point of care, where the testing of diseases is performed at the bedside, *i.e.* near the patient, using portable or mobile devices that give an immediate diagnosis, which in turn allows immediate treatment (Wang *et al.*, 2017). There is interest in applying NMs in devices for point of care diagnostics, as they have characteristics (such as shape, size, biocompatibility, thermal and electrical conductivity, magnetism, and fluorescence) that can improve these detecting systems (Quesada-Gonzalez and Merkoci, 2018). Gold nanoparticles (AuNPs) are an example of a type of NM that is being developed as a way of increasing the sensitivity of electrical biosensors for point of care diagnostics since they increase their surface area (Bayford et al., 2017). Recently, a biosensor was created with AuNPs with enhanced fluorescence to allow the detection of immunoglobulin

concentration changes in urine samples in a few minutes. This very sensitive technique can allow the detection of even minimal changes, which can be indicative of renal injuries (Della Ventura *et al.*, 2019).

1.1.2 THERAPY

Drug delivery systems are ways of transporting and releasing, in a specific cell or tissue, controlled quantities of drugs for therapeutic effects. This allows the increase of drug efficiency, as well as reduction of toxicity and optimization of kinetics and dynamics (Medina-Reyes *et al.*, 2017). NMs can be used in this context, either for drug encapsulation or for attachment of drugs to the surface of the NMs, and both can be used to induce a controlled release of the drug at the target tissues (Patra *et al.*, 2018). This type of delivery system can not only extend the time during which the drugs are in the bloodstream, increasing the passage of drugs to tissues (Medina-Reyes *et al.*, 2017) but also, due to their small size, facilitate the uptake by diseased cells in the target tissue, resulting in higher efficiency and decreased side effects (Patra *et al.*, 2018)

The replacement of damaged tissues and organs by constructs made up of cells and biomaterials is the main goal of tissue engineering (Padmanabhan and Kyriakides, 2015). To this end, the creation of scaffolds that mimic the original tissues in their biochemical, mechanical, and electrical properties is very important (Kim *et al.*, 2014). These scaffolds are the mechanical support for the cells so that they can differentiate in multiple cell types and develop the 3D aspects of tissue systems (Bhattacharjee and Brayden, 2015). NMs can be used to make up this scaffolding, due to their high surface area/volume ratio, that enable higher cell attachment and activity, efficient bioactive molecular loading, and incorporation of functional components (Jin *et al.*, 2017). An example of the latter can be seen in a study by Yun et al. (2009), where carbon nanotubes were functionalized to provide a more hydrophilic surface, which increased fibroblast adhesion to the scaffold (Yun *et al.*, 2009). A schematic example of scaffolding can be seen in figure 1.

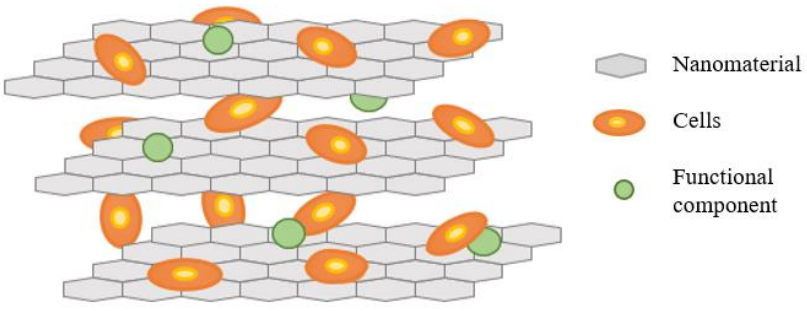

Figure 1 – Scaffolding created using nanomaterials for cell fixation with functional components for tissue engineering. The functional components can be growth factors or compounds that alter the properties of NMs (like charge).

1.2 BIOKINETICS OF NMS

To be able to understand the ways that NMs can induce toxicity to the human being it is important to understand their biokinetics and how the organism alters the original characteristics of NMs.

1.2.1 ABSORPTION

Inhalation, ingestion, and dermal exposure are the three most common pathways for the absorption of NMs (Warheit and Donner, 2015). NMs for biomedical applications can also be injected directly into the bloodstream (Dusinska *et al.*, 2015).

Upon inhalation, NMs tend to deposit throughout the respiratory tract, and the smallest ones (10 to 20 nm) can reach the alveoli and deposit (Bierkandt *et al.*, 2018). Inhaled NMs generally have low systemic availability, as most types form aggregates that are taken up by macrophages when they reach the alveoli (Landsiedel *et al.*, 2012, Gebel *et al.*, 2014). However, this phagocytosis is not as efficient as with micromaterials, allowing NMs to persist for a longer time in the lung and increasing the probability of crossing the epithelial barrier of the alveoli and then, possibly, the air-blood barrier (Puisney *et al.*, 2018).

The oral administration of nanocarriers for drug delivery offers increased bioavailability to drugs, since the NMs act as a protection from the gastrointestinal environment, that could easily degrade the drugs (Ciappellano *et al.*, 2016). This is contrasting with the fact that, generally, only about 1% of the ingested dose of NMs is absorbed from the gastrointestinal tract (mostly in the small intestine), and studies in mice show that the absorbed fractions mostly reach the liver and the spleen, while the remaining part is excreted with the feces (Landsiedel *et al.*, 2012, Kermanizadeh *et al.*, 2015a). Despite this poor absorption, NMs can help drug delivery not only because of the protection that NMs provide, but also because they prolong the period during which the drug is being absorbed through the intestinal epithelium. This happens because the adhesive properties of NMs allow for the gradient of concentration of the drug between the nanocarrier and the gut mucosa to be maintained, which is one of the most important factors in drug absorption (Shahbazi and Santos, 2013). Gastrointestinal absorption is affected by the characteristics of NMs, such as size and charge, and also by gastrointestinal factors, such as variations in pH, intestinal microbiota, and enzymatic and mucosal secretions (Pietroiusti *et al.*, 2017).

Topical administration and subsequent dermal absorption of products containing NMs can also occur. Studies are showing that there can be unwanted absorption of the nanoparticles through the skin (McSweeney, 2016), which can provoke the activation of an immune response and possible toxicity in the liver, spleen, and other organs (Saifi *et al.*,

2018). Nevertheless, this route seems to be less relevant, being enhanced, however, if the skin has suffered some damage (Landsiedel *et al.*, 2012).

1.2.2 DISTRIBUTION

NMs can suffer lymphatic transport, which will influence their overall distribution throughout the organism (Li *et al.*, 2017). It is common for NMs to be taken up by macrophages and can thus be accumulated primarily in the liver and then in the spleen, lymph nodes, and bone marrow, as these are the organs with the highest abundance of macrophages (Yuan *et al.*, 2019). These organs have a leaky endothelial barrier, which promotes the entry of NMs. The capacity to permeate the blood-brain barrier is known for some NMs, and it is thought that the adsorbed proteins on their surface can alter the capacity of adherence to the endothelial cells and endocytosis of NMs through this barrier (Landsiedel *et al.*, 2012). Accumulation in the brain can also occur due to uptake by the sensory nerve ends in the airway epithelia (Landsiedel *et al.*, 2012). Some studies are showing that there is a biodistribution of NMs to the placenta and fetus. In one study, 10-day pregnant mice were orally given 30 nm zinc oxide NPs (ZnO NPs) at 20, 60, 180, or 540 mg/kg, and the distribution of the NPs was assessed at 10.5 and 17.5 days of gestation by quantification of zinc with inductively coupled plasma mass spectrometry (Chen *et al.*, 2020). The results showed the presence of significantly higher levels of zinc in the uterus, placenta, and fetus for the 540 mg/kg dose, which indicates distribution through the placental barrier of ZnO NPs (Chen *et al.*, 2020).

1.2.3 METABOLISM

NMs metabolism encompasses any process that alters the original form of the NMs, that is, their physicochemical properties, and it is an area for which information is still lacking (Yuan *et al.*, 2019). NMs can be taken up by phagocytic cells, such as monocytes and macrophages. After phagocytosis, NMs can be degraded inside of the lysosomes or, if this does not happen, the phagocytic cells with the NMs can be sequestered by the liver or the spleen, which can then lead to accumulation in these organs (Zhang *et al.*, 2016). Metabolism can also occur in the hepatocytes by enzyme-catalytic biodegradation, due to a high abundance of phase I and II enzymes in the liver (Wang *et al.*, 2013). In phase I, functional groups are created on the coating compounds in the surface of the NM, by reactions like hydrolysis or oxidations, that increase the reactivity and polarity of NM. Then, in phase II, conjugation with endogenous compounds can occur, increasing water solubility and diminishing reactivity, thus promoting excretion (Lungu *et al.*, 2019). However, inert NMs, like gold, tend to accumulate in the liver without being metabolized (Wang *et al.*, 2013).

Generally, inorganic NMs, such as gold and quantum dots, are very stable in the organism and persist during a long period of time, resisting biodegradation, contrary to organic NMs (liposomes and polymer conjugates for example) that degrade rapidly and whose metabolic products are excreted through the bile or urine (Wilhelm *et al.*, 2016, Yuan *et al.*, 2019). After internalization into cells, the coating materials that are commonly applied to NMs surface can be cleaved off and degraded separately from the core, inside endosomes, such as peptide cleavage by cathepsin L protease of peptide-coated NMs (Li *et al.*, 2010). Figure 2 resumes the general mechanisms of NMs' metabolism.

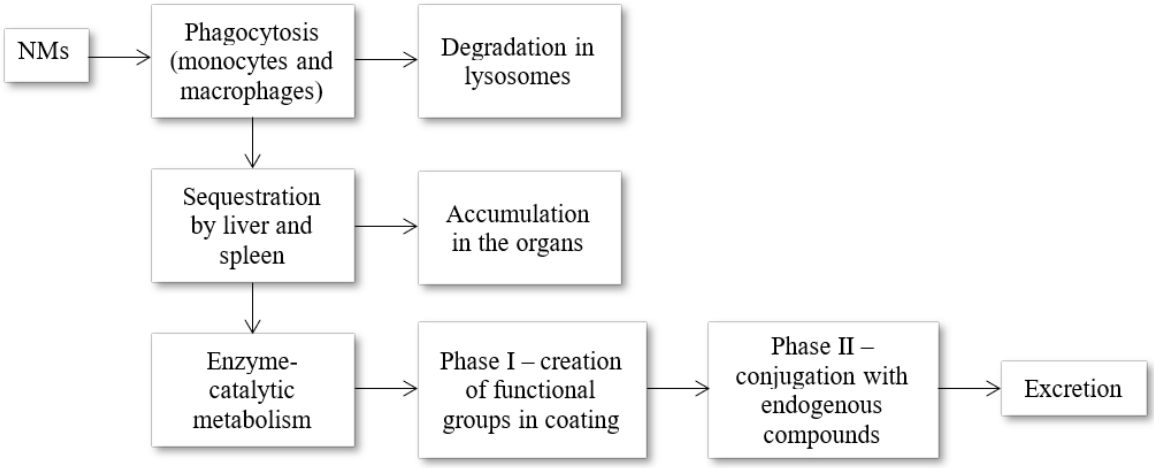

Figure 2 – Metabolism of NMs.

1.2.4 EXCRETION

The excretion of absorbed NMs is mainly carried out through the bile and the kidneys. Kidney excretion mostly relies on glomerular filtration for the clearance of compounds and it is restricted to materials with very small hydrodynamic diameters (Yu and Zheng, 2015). Therefore, particles with less than 5 nm can be excreted by this route (Longmire *et al.*, 2008). The glomerular membrane has proteoglycans that confer a negative charge to this barrier, making cationic NMs filtration faster (Liang *et al.*, 2016).

Hepatobiliary excretion is slower but is the preferable course for the elimination of NMs that are too large for urinary clearance (Yuan *et al.*, 2019). NMs that escape the Kupffer cells reach the hepatocytes in the liver and can be then taken up by these cells (Zhang *et al.*, 2016). This is a process that is enhanced if the material has a positive surface charge, contrary to Kupffer cell uptake, which is enhanced with negative surface charges (Wang *et al.*, 2015). Hepatic uptake was observed and it is likely since positive NMs bind with immunoglobulin A and apolipoprotein E, which enhances uptake by hepatocytes (Cheng *et al.*, 2012). Kupffer cell uptake happens since these cells have scavenger receptors in their membrane that bind molecules with a negative charge (Poelstra *et al.*, 2012). In the

hepatocytes, the NMs can be metabolized (or not), and the original NM, or its degradation products, are afterward excreted in the bile (Yuan *et al.*, 2019).

1.3 FACTORS THAT AFFECT THE BIOKINETICS OF NMS

It is known that properties like surface charge, size, and hydrophobicity can alter the way compounds interact with the organism, and this is no less true to NMs, as evidenced by a great number of studies described below.

1.3.1 HYDROPHOBICITY AND HYDROPHILICITY OF THE SURFACE

Hydrophobicity and hydrophilicity have a strong influence on the surface interactions of NMs, as with the increase of hydrophobicity there is usually a higher formation of aggregates (Zhu *et al.*, 2013). This will change the physicochemical characteristics of NMs, altering parameters like size and solubility, which will affect cellular uptake and distribution through the organism. Most of the time, the aggregation will decrease absorption and toxicity (Hussain *et al.*, 2014). Aggregate formation will also slow down the excretion of the NMs (Zhu *et al.*, 2013). Besides this, it is known that the more hydrophobic the NM surface is, the more proteins will bind to its surface, and that this hydrophobicity also changes the type of the adsorbed proteins (Aggarwal *et al.*, 2009). For example, hydrophobic NMs show higher binding to apolipoproteins and blood proteins like opsins, which increases macrophage uptake (Chen *et al.*, 2017). The combination of the adsorbed proteins and other biomolecules (like lipids and sugars) present in fluids leads to the formation of a protein corona (Monopoli *et al.*, 2012, Vilanova *et al.*, 2016). The presence of this corona changes the way the NM interacts with the components of the organism, altering, for example, the immunological response (Neagu *et al.*, 2017). These changes can either increase recognition by immune cells, favoring later elimination; camouflage the NM and decrease the immune recognition; or alter the conformation of proteins adsorbed, which can in turn signal to the immune cells, leading to the initiation of an inflammatory response (Boraschi *et al.*, 2017).

1.3.2 SURFACE CHARGE

Surface charge of NMs is determinant in their kinetics and toxicity. Neutral surfaced NMs decrease opsonization and removal from the bloodstream, as well as interactions with cell surface (Landsiedel *et al.*, 2012, Gebel *et al.*, 2014). On the other hand, a positive charge increases cellular uptake, as it favors adherence to the anionic cell surface, and interactions with genetic material, which can increase the potential toxicity of the NMs (Zhu *et al.*, 2013, Saifi *et al.*, 2018). The surface charge can influence the formation of agglomerates and aggregates, altering the physicochemical properties of the NMs (Pietroiusti *et al.*, 2018). Anionic surfaced NMs are usually taken up by phagocytic cells, diminishing their toxicity, since they are taken out of circulation and excreted and, hence, cannot affect cells and

tissues (Frohlich, 2012). In terms of uptake through the gastrointestinal tract, cationic surfaces promote absorption (Landsiedel *et al.*, 2012).

1.3.3 SIZE

NMs have, generally, a size under 100 nm. This small size translates into a higher surface area to volume ratio, increasing the reactivity of NMs towards biomolecules and cells (Saifi *et al.*, 2018). Even usually inert materials, for example, gold, when at the nanoscale, end up having reactive catalytic functions (Caputo *et al.*, 2014). Size is one of the important aspects when considering the mechanism of NMs' cell uptake. NMs of a few nanometers can only penetrate the cytoplasmatic barrier directly if they have appropriate surface properties. To be able to undergo endocytosis, the NM needs to have the size of the corresponding endocytic portal (Zhu *et al.*, 2013). Once inside the cells, the NMs are kept for a longer period, which can lead to accumulation and toxic effects in the long run (Rivera Gil *et al.*, 2010), and have a higher likelihood of interacting with cell components, such as mitochondria, lysosomes, nucleus and genetic material (Saifi *et al.*, 2018). The size also plays an important role in penetration through the skin, as only NMs, with their small size, have the potential of going through the stratum corneum (Kermanizadeh *et al.*, 2015a). In figure 3 a summary of the main biokinetic processes influence by physicochemical changes in the NMs' physicochemical properties is present.

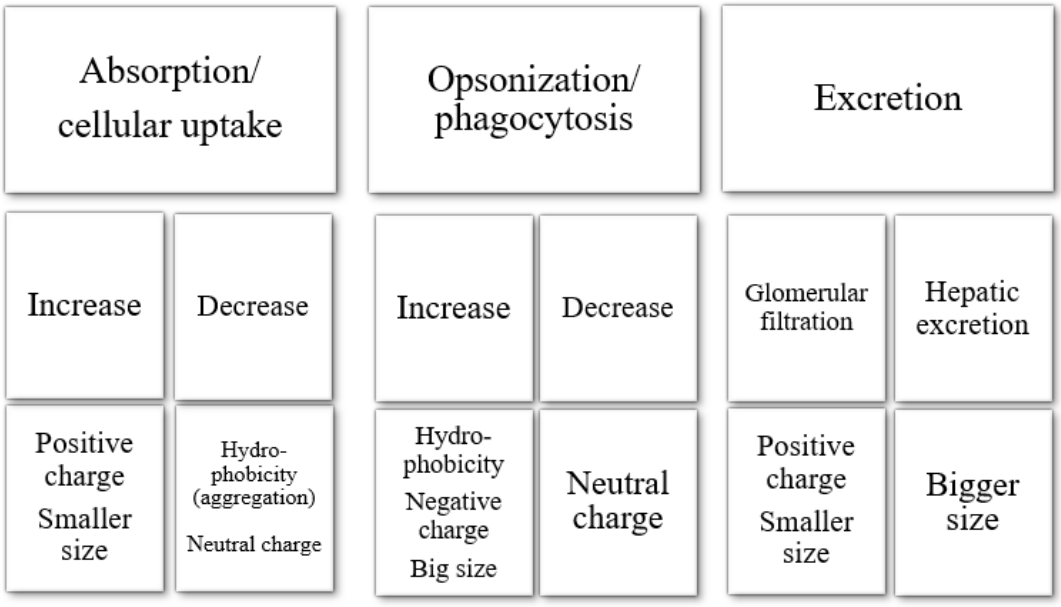

Figure 3 – Biokinetic components altered by nanomaterials characteristics.

1.4 MECHANISMS OF TOXICITY OF NMS

Oxidative stress, inflammatory effects, and genotoxicity are primarily agreed as the main mechanisms of the toxicity of NMs.

1.4.1 OXIDATIVE STRESS AND MITOCHONDRIAL DAMAGE

Reactive oxygen species (ROS) production is one of the main and most frequently reported mechanisms of toxicity of NMs. Typically, the levels of ROS are in balance with the antioxidant system of the cells, comprised of compounds like glutathione (GSH) and antioxidant enzymes, but when an imbalance occurs it leads to oxidative stress (Lv *et al.*, 2015). If this stress is not reversed, it can cause inflammation, adaptative immune responses, initiation of apoptosis/necrosis, and oxidative damage to DNA, lipids, and proteins (Kermanizadeh *et al.*, 2015b).

NMs can increase ROS levels directly, due to their surface properties, or by influencing their intracellular production (Saifi *et al.*, 2018). Direct production has been mostly linked to metal or metal oxide NMs, which produce free radicals that originate ROS (Chen *et al.*, 2018). On the other hand, NMs can interfere, for example, with the electron transport chain by increasing the permeability of the mitochondrial membrane. This process will allow the free oxygen radicals, that are usually quenched during the electron transport chain, to leak to the outside of the mitochondria, causing oxidative stress in the cell (Bhattacharjee and Brayden, 2015). The interference with the mitochondrial membrane, combined with a significant alteration of mitochondrial proteins, will also end up hindering processes like the production of ATP, the citric acid cycle, and β-oxidation of fatty acids (Chen *et al.*, 2018, Zhang *et al.*, 2018a). This dysregulation of the mitochondria can also lead to the release of calcium to the cytoplasm, and, at high concentrations, this can result in the activation of apoptotic and/or necrotic pathways for cell death (Bhattacharjee and Brayden, 2015).

1.4.2 INFLAMMATORY EFFECT

Besides oxidative stress, NMs can induce an inflammatory response, either by promoting the production of proinflammatory cytokines or by activating inflammasomes (Pietroiusti *et al.*, 2018). It is the interaction of the NMs with immune cells (such as monocytes, neutrophils, macrophages, and others) in the circulation that potentiates the release of a cascade of cytokines, including interleukin 1 beta, interleukin 6, tumor necrosis factor-alpha and interleukin 8, that cause inflammation (Saifi *et al.*, 2018). Inflammasomes are intracellular multiprotein complexes that are produced by phagocytosis of NMs and rupture of the phagosome or by the interaction of the cell membrane with the NMs. Activation of these inflammasomes will lead to the activation of proinflammatory cytokines and, therefore, lead to their increase in the organism and, therefore, inflammation (Padmanabhan and Kyriakides, 2015).

It has also been shown that activation of inflammasomes in macrophages can result in pyroptosis, a type of programmed cell death (Leso *et al.*, 2018). It starts with the assembly

of inflammasomes, which will form large structures called pyroptosomes that have an apoptosis-associated speck-like protein containing a C-terminal caspase recruitment domain (Simard *et al.*, 2015). Pyroptosis-induced cell death shares characteristics with apoptosis (nuclear condensation and DNA fragmentation) and with necrosis (rupture of the cellular membrane and release of the intracellular contents) (Wang and Tang, 2018).

Lastly, NMs can also activate mast cells and this can end up in allergic inflammation (Smith *et al.*, 2014).

1.4.3 GENOTOXICITY

DNA damage induced by NMs can be primary, direct or indirect, and secondary (Saifi *et al.*, 2018). Primary direct damage occurs when the NM has the capacity of reaching the nucleus and, once there, bind, chemically or physically, with the DNA molecule and provoke structural damage (Lorscheidt and Lamprecht, 2016). The entrance into the nucleus can occur either by nuclear pores or during mitosis since during this process the nuclear membrane breaks down. The nuclear pores have an hourglass shape and a dynamic size, which allows the entrance of NMs with size up to 90 nm (Frohlich, 2012). The major indirect genotoxic mechanism is oxidative stress, as ROS attack DNA and cause oxidative injury (Dusinska *et al.*, 2017). Primary indirect damage can also occur when the proteins related to the DNA lose or have a restricted function after NM binding (Lorscheidt and Lamprecht, 2016). Other mechanisms, such as interaction with the mitotic spindle or its components and interference with cell cycle checkpoint functions can also have an indirect impact on the genetic material (Gebel *et al.*, 2014). Secondary mechanisms of DNA damage are mostly associated with chronic inflammation from activation or recruitment of immune cells, such as macrophages and neutrophils, and consequent production of extracellular ROS (Dusinska *et al.*, 2017, Saifi *et al.*, 2018). Unrepaired DNA damage can activate pathways that lead to apoptosis or changes in DNA that result in mutations, which can then culminate in cancer or heritable diseases (Lorscheidt and Lamprecht, 2016). Figure 4 illustrates the possible ways that NMs can cause toxicity in living organisms.

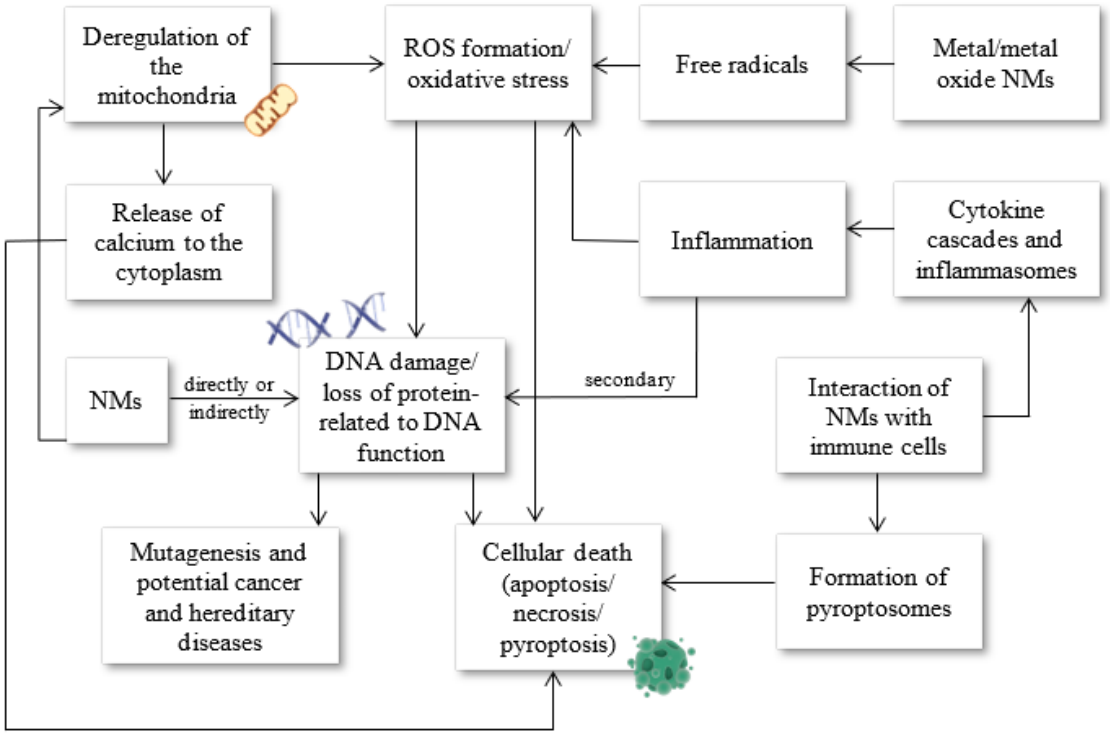

Figure 4 – Mechanisms of toxicity of NMs.

It is important to note that most of the toxicity mechanisms described (oxidative stress, inflammation, and genotoxicity) can be enhanced or diminished according to the physical and chemical properties of the NM, as well as due to the possible corona that is formed in contact with the biological system. For example, positively charged NMs have a higher probability of provoking disruption of plasma membrane integrity, of damaging the mitochondria and lysosomes, and of increasing the formation of autophagosomes as compared to the negatively charged NMs, due to their higher interaction with biological membranes (Frohlich, 2012).

It is also important to characterize the underlying mechanisms of each NMs' toxicity, and, for that, several techniques can be used. One of the most important is metabolomics, which has been increasingly used, due to its many advantages, including its high sensitivity.

1.5 METABOLOMICS

The metabolome is the qualitative and quantitative collection of all low molecular weight molecules in an sample, known as metabolites, that are usually organic compounds (amino and fatty acids, vitamins and lipids for example), with a wide range of physicochemical properties that are responsible for several cellular processes, such as maintenance, growth and overall normal function of the organism. The metabolome varies in size depending on the organism (Dunn and Ellis, 2005). Metabolites can be endogenous (from cells of the

organism) or exogenous (derived from microorganisms, xenobiotics, diet, and others). The focus of metabolomics is to identify and quantify all the metabolites present in the organism in a high-throughput manner. This poses some challenges due to the chemical and concentration variability of the metabolites as well as the fact that not every metabolite is present in every tissue or biofluid (Wang *et al.*, 2010).

The use of metabolomics to study NM induced toxicity allows an analysis of changes in the metabolome of cells, tissues, and biofluids, which can give information on potential nanotoxicity biomarkers, elucidate mechanisms of action, and analysis of pathways of interest that can be difficult to measure using traditional methods, since these are less sensitive and less specific (Schnackenberg *et al.*, 2012).

The two main analytical platforms used in these types of studies are nuclear magnetic resonance (NMR) spectroscopy and mass spectrometry (MS), where the latter can be coupled with chromatographic methods, and both can be combined to complement metabolite coverage (Amberg *et al.*, 2017). Metabolomics allows the identification of metabolites and metabolic pathways that are associated with specific phenotypes as well as the discovery of biomarkers of toxicity or disease, and it can be done in an untargeted manner, which analyzes all the metabolites in a sample, or targeted manner, where specific metabolites are selected for study (Johnson *et al.*, 2016). Additionally, there is also metabolomic fingerprinting (analysis of changes in intracellular metabolites by comparison of metabolite patterns) or metabolomic footprinting (analysis of extracellular metabolites secreted from cells or metabolites of the cellular medium not used by the cells) (Frohlich, 2017).

1.5.1 ANALYTICAL PLATFORMS

NMR spectroscopy uses electromagnetic radiation of a resonance frequency with enough energy to induce the transition of spins between different energy levels from a magnetic nucleus when placed in a magnetic field (Hore, 2015). In MS, the mass/charge ratio (m/z) of ions, formed by induced loss or gain of a charge by a neutral species, provide information that can be used to determine the identity of a molecule and its fragments. The complex sample of metabolites can be directly injected into an MS or can go through a chromatographic separation process before MS analysis (Johnson *et al.*, 2016).

1.5.2 UNTARGETED VERSUS TARGETED METABOLOMICS

The main goal of untargeted metabolomics is to study all the metabolites in a sample. This technique can be used to identify and characterize unknown metabolites and to measure statistically relevant relative changes in metabolite levels between samples by comparing integrated mass ion intensities (Vinayavekhin and Saghatelian, 2010). In targeted metabolomics, the studies are hypothesis testing and focus on a specific number of

metabolites, related by either class or function, and allow the absolute quantification of the concentration of the metabolites under analysis by the use of internal standards, that are generally isotope analogs of those metabolites (Dunn *et al.*, 2011).

Overall, each method, targeted and untargeted, has strengths and shortcomings. Untargeted metabolomics does not require previous knowledge of relevant metabolites, being useful in finding new mechanisms and in identifying chemically unknown metabolites, though this is only a semi-quantitative method that generates an enormous amount of complex data and that requires validation of any identified metabolites (Menni *et al.*, 2017, Ribbenstedt *et al.*, 2018). In contrast, targeted metabolomics, that focuses on only some metabolites, has higher sensitivity and precision (and therefore lower detection limits), easily identifies metabolites and gives absolute quantification, but does not allow the discovery of unknown compounds and has limited metabolome coverage, which can lead to the overlooking of metabolomic responses of interest (Menni *et al.*, 2017, Ribbenstedt *et al.*, 2018).

1.5.3 FINGERPRINTING VERSUS FOOTPRINTING

Fingerprinting metabolomics studies the intracellular metabolites in a high-throughput manner, where the main objective is not to generate quantitative data or to identify each metabolite, but to compare fingerprints (patterns) of metabolites that change due to disease or toxic exposure using statistical tools like hierarchical clustering or principal component analysis (PCA) (Dettmer and Hammock, 2004). Global intracellular fingerprinting is difficult to obtain with one method and it is a time-consuming technique that requires robust methods for fast quenching of metabolism and extraction from cells since there is a rapid metabolite turnover (Kim *et al.*, 2010). On the other hand, metabolic footprinting analyzes the extracellular metabolites that are secreted by the cells or tissues to the external environment plus those metabolites that the cells or tissues do not uptake, which reflect the cellular metabolic activity. When using this technique, the need for rapid quenching disappears since the turnover of the metabolites is slower in the external environment (Kell *et al.*, 2005).

1.5.4 METABOLOMICS IN NANOTOXICOLOGY

When compared to classical toxicity tests, metabolomics is more sensitive, non or less invasive (since urine, serum, and saliva can be used), is less time consuming, and gives a more complete view of biochemical variations, which makes it useful in toxicity assessment of NMs (Lin *et al.*, 2012). Cell metabolomics can be integrated with traditional *in vitro* toxicity endpoints to discover associations between metabolic profile alterations and NM induced mechanisms of cytotoxicity, like oxidative stress, inflammation, and cell viability,

and footprinting techniques can give indirect information about physiological status and phenotype of cells (Lv *et al.*, 2015).

An example of a study that comprises the methods explained above is the one performed by Lindeque et al. (2018) that analyzes the endo and exometabolome of human caucasian hepatocyte carcinoma (HepG2) cells exposed to three differently coated AuNPs, poly-(sodiumsterene sulfonate) (PSSNa-AuNPs, 0.25 nM), poly-vinylpyrrolidone (PVP-AuNPs, 0.25 nM) and citrate (Cit-AuNPs, 0.5 nM), for 3 h. The exometabolome was analyzed by NMR spectrometry. For the endometabolome study, untargeted metabolomics was performed with gas chromatography coupled with mass spectrometry (GC-MS), and targeted analysis of amino acids and acylcarnitines was conducted by liquid chromatography coupled with tandem mass spectrometry LC-MS/MS (triple quadrupole). The comparison of the exometabolome from the medium of exposed cells and of controls showed increased concentrations of several metabolites for PSSNa-AuNPs and PVP-AuNPs. For PSSNa-AuNPs, moderate differences were detected for three metabolites (proline, glutamine, and lactate), which could be related to decreased ATP production (lactate) and, consequently, higher amino acid metabolism (proline and glutamine). PVP-AuNP exposure, however, showed a significant increase in amino acids (proline, glutamic acid, glutamine, and arginine) and of compounds related to phospholipid metabolism (choline and myo-inositol). The increased proline was associated with the release of PVP monomers from the coating of the AuNP, which are similar to proline, and this is why its pathways products (glutamic acid, glutamine, and arginine) were also increased. Cit-AuNPs increased concentrations of extracellular lactic acid, thus interfering with ATP production (Lindeque *et al.*, 2018). When looking at the endometabolome results, several metabolites were identified, linked to amino acid, carbohydrate, lipid, energy, and acylcarnitine metabolisms. In both untargeted and targeted metabolomics, almost all metabolite concentrations were decreased, which was hypothesized to be related to metabolite binding to the ligands on the surface of AuNPs, but the authors noted that more studies are needed to validate this hypothesis Overall, PVP-AuNPs were the ones that interfered more with the intracellular metabolome, relating to its higher internalization rate. Although every coating led to a decrease in intracellular metabolites, only PSSNa-AuNPs and Cit-AuNPs affected ATP production (Lindeque *et al.*, 2018).

Our group carried out a metabolomics study to assess the mechanism of toxicity of differently shaped AuNPs (Enea *et al.*, 2019a), which had already been shown by others in *in vitro* studies (Favi *et al.*, 2015), but only at higher concentrations and without demonstrating the mechanism behind the different effects. In the work by Enea et al. (2019a), 40 nm gold nanospheres and 47 nm gold nanostars were administered intravenously to rats (1.33×10^{11} AuNPs/kg). After 24 h, the liver was removed for

evaluation of biomarkers of toxicity (levels of ATP, GSH and oxidized glutathione, GSSG) and metabolomic analysis. The rats showed no behavioral or physical changes. Hepatic GSH and GSH/GSSG ratio levels increased after administration of both types of NPs and ATP levels did not change. Despite this apparent lack of toxicity or differences between the two differently shaped AuNPs, when the metabolomic assay was performed this was not the case. Both AuNPs produced alterations in several metabolic pathways, namely protein, fatty acid, GSH, and purine/pyrimidine metabolism, changes that preceded toxicity. The nanospheres had a stronger and significant effect on the fatty acid synthesis and nanostars on protein synthesis. This shows the higher sensitivity of metabolomic studies in discriminating responses to different NPs, which could not be noticed in conventional *in vitro* assays and possibly predict toxic events, which proves that it is a great asset in nanotoxicological studies. They can, however, also detect alterations that have no consequence in the phenotype of cells or alterations related to adaptative responses to damage, which is a shortcoming of these techniques. (Enea *et al.*, 2019a).

Inorganic nanomaterials are of great interest in medicine, and because of this, it is important to understand how they behave and interact with the human organism. Metabolomics can be successfully used to uncover metabolic pathways of nanotoxicity, but there is still the need to continue developing metabolomics research to further identify more mechanisms and biomarkers of NMs toxicity.

1.6 NANOPARTICLES

1.6.1 GOLD NANOPARTICLES

AuNPs are important NPs that have a wide spectrum of applications. Their physicochemical properties are extremely useful, mainly their redox behavior, the ability to quench fluorescence, and the effect of surface plasmon resonance (Yeh *et al.*, 2012). For their biological uses, the most important characteristics are the great biocompatibility and the large surface area, which allows the conjugation and functionalization of their surface with a variety of molecules, to various ends (Khan *et al.*, 2014). Synthesis of AuNPs can be performed through many methods, but the most commonly used is the chemical reduction of gold chloride with sodium citrate devised by Turkevich and improved later by Frens, who changed the ratios of the compounds, which resulted in spherical AuNPs with control over size (Frens, 1973).

AuNPs have been demonstrated to be of great use in medicine. This is both due to their advantages on imaging techniques for diagnosis, like computed tomography imaging, but also in therapy, with their potential for drug delivery systems and photothermal therapy (Panahi *et al.*, 2017). They can be widely applicable as biosensors for several different

compounds, from metals to toxins. There are different types of sensors such as colorimetric or fluorescence sensors (Elahi *et al.*, 2018). Applications in cancer are currently being developed since AuNPs, due to their small size, can penetrate and deposit in tumors and can also bind to biomolecules and drugs for target delivery (Peng and Liang, 2019).

Several studies have been performed to assess AuNPs' toxicity and, generally, these particles have been found to exert little toxicity, particularly those that are smaller and with a negative surface charge, the latter possibly being related with cells having a negative membrane, leading to a weak interaction with anionic AuNPs (Goodman *et al.*, 2004). This, however, cannot assure the safety of the use of AuNPs since they can have long term effects, as they accumulate in the body, particularly in the liver and spleen (Yuan *et al.*, 2019). Therefore, and similarly to the aforementioned NPs, further studies need to be conducted to assure the safe use of AuNPs (Adewale *et al.*, 2019).

1.6.2 SELENIUM NANOPARTICLES

Selenium is a semi-metal, belonging to the same family of sulfur and oxygen. It is essential for the organism since it is a vital component of selenoproteins, such as glutathione peroxidase, that play an important part in several body functions (Mehdi *et al.*, 2013). Nanosized selenium or selenium nanoparticles (SeNPs) have been gaining attention in various fields, such as in electronics, optics, and medicine. They can be synthesized through chemical (e.g. acid decomposition) or physical (e.g. UV radiation) methods but biosynthesis, using bacteria, fungi, or plants, has been growing in popularity, since these methods produce stable SeNPs that do not aggregate, and it is cheaper and eco-friendlier (Wadhwani *et al.*, 2016). When compared with some selenium compounds, namely selenite, Se-methylselenocysteine, and selenomethionine, SeNPs have overall lower toxicity (Zhang *et al.*, 2005, Zhang and Spallholz, 2011).

In terms of nanomedicine applications, SeNPs have gained increased interest. They have high bioavailability, provide a sustained and targeted release of selenium, which leads to the accumulation of this element in tumoral sites and reduction of distribution to healthy tissue (Guan *et al.*, 2018). In fact, one major area where SeNPs show incredible promise is in anticancer treatment. In general terms, SeNPs suffer endocytosis and, when inside cancerous cells, have a prooxidative effect because of the redox imbalance. This will lead to mitochondrial leakage and cell stress, ending up with the activation of apoptotic pathways. SeNPs will also interfere with pathways related to oncogenic signaling (like the vascular endothelial growth factor pathway), which decreases cell proliferation and growth (Khurana *et al.*, 2019). Functionalization of the surface of SeNPs, with organic and inorganic compounds, can impede their aggregation and decrease toxicity while also enhancing cell uptake. Targeting can be achieved through functionalization as well, using biomolecules,

like ligands and antibodies (Maiyo and Singh, 2017). Studies have demonstrated the use of functionalized SeNPs in delivering doxorubicin and doxorubicin compacted with siRNA to cancerous cells, with great results in selective uptake and cytotoxicity towards these cells, attesting to the capacity of SeNPs to be used as drug and gene delivery agents in anticancer treatment (Huang *et al.*, 2013, Xia *et al.*, 2018).

Besides their application in cancer, SeNPs have antibacterial and antiviral effects, especially biogenic SeNPs. Cremonini et al. (2016) demonstrated inhibition of the growth of *Pseudomonas aeruginosa* using SeNPs synthesized by gram-positive *Bacillus mycoides* and gram-negative *Stenotrophomonas maltophilia*, with no effects on human cells (Cremonini *et al.*, 2016). In another study by Ramya et al. (2015), the SeNPs synthesized by *Streptomyces minutiscleroticus* demonstrated antioxidant and anti-biofilm activities that were concentration-dependent, as well as effective antiviral activity against type-1 dengue virus, via reducing of growth (Ramya *et al.*, 2015).

1.6.3 SILVER NANOPARTICLES

Silver nanoparticles (AgNPs) also belong to the group of metal nanoparticles. Their characteristics, including being a great catalytic, having high sensitivity for optical sensors due to the surface plasmon resonance effect, and having a high surface area, are what make these NPs so desirable in many fields, including medicine (Abbasi *et al.*, 2016).

It is well established that AgNPs have strong antimicrobial activity. Generally, these particles accumulate on, and penetrate the cellular wall and membrane, binding with the biomolecules on the membranes and inside, causing changes in membrane permeability and essential cellular processes, like the respiratory chain or protein synthesis, which eventually leads to bacterial cell death (Tang and Zheng, 2018). AgNPs also release silver ions, that lower the cellular pH and lead to the formation of free radicals. Silver ions bind with sulfur and thiol groups of proteins and peptides, namely GSH, eventually culminating in oxidative stress (Naik and Kowshik, 2017). AgNPs are also being used to improve the efficiency of cancer treatments by combining them with anticancer drugs, that are used in smaller concentrations and with fewer side effects for non-cancerous cells (Yuan *et al.*, 2018). These nanoparticles have also been used in diagnosis and imaging, both due to their efficiency at absorbing and scattering light and also because they can be used for fluorescent labeling (Lee and Jun, 2019).

Despite all these uses, AgNPs must be used with care since they can have the same lethal effects on human healthy cells as those that they have on bacteria. AgNPs can interfere with the proliferation and be cytotoxic, effects that are dependent on coating and size (Souza *et al.*, 2018). Silver deposits from AgNPs exposure are common in many organs, like the liver, kidney, or the skin, where it provokes discoloration to a blue-gray color, a phenomenon

called argyria (Hadrup and Lam, 2014). It is also important to note the possible ecotoxic side effects that particulate silver can have on different species. Hence, it is crucial to keep studying AgNPs to close current knowledge gaps and to increase the safety of its use (Du *et al.*, 2018).

2. OBJECTIVES

As seen in the previous section, NMs have a wide range of applications, mainly in nanomedicine where they can improve classical therapeutic and diagnostic approaches. However, their mechanisms of toxicity are not well defined. Bearing this in mind, it is important to develop techniques that allow the detailed study of the possible alterations that NMs can cause to organisms.

In this work, the focus was to evaluate metabolomic changes in primary rat hepatocytes after exposure to six types of nanoparticles at non-toxic concentrations. The nanoparticles chosen were citrate coated nanospheres of gold (12, 40, and 60 nm), 11-mercaptoundecanoic acid (MUA) coated nanostars of gold (60 nm), citrate coated nanostars of silver (200 nm), and glucose coated nanospheres of selenium (300 nm). Ultimately, this study aimed to determine if there are, at non-cytotoxic concentrations, changes in the cells that cannot be detected in the conventional cytotoxic assays. For this, metabolomics was chosen, since it has the potential to detect small changes in the metabolome due to its high sensitivity.

To this end, the procedures aimed at:

(1) Assessing the highest concentration of the different NPs that caused no toxicity to primary rat hepatocytes via two cytotoxicity assays (neutral red and MTT).

(2) Studying the metabolic changes induced by the different NPs at non-cytotoxic concentrations via metabolomics performed with GC-MS.

3. MATERIALS AND METHODS

3.1 CHEMICALS AND REAGENTS

All chemicals used in this study were of analytical grade and high purity unless stated otherwise. All the chemicals were obtained from Sigma-Aldrich (Missouri, USA). Cell culture reagents were purchased from Gibco (Alfagene, Lisbon, Portugal). For the NPs synthesis, all chemicals and reagents were used without further purification unless indicated otherwise. Gold (III) chloride 30% wt solution (99.99%), 11-mercaptoundecanoic acid (MUA, 95%), silver nitrate (99.9999%), neutral hydroxylamine 50% wt (HA, 99.9999%), sodium selenite (98%) and D-(+)-glucose (99.5%) were from Sigma-Aldrich (Missouri, USA). Trisodium citrate dihydrate (99%) was from Merck (Darmstadt, Germany) and sodium hydroxide (98.7%) from Fisher Scientific (Hampton, New Hampshire, USA).

3.2 SYNTHESIS AND CHARACTERIZATION OF NPS

The synthesis and characterization of all NPs were kindly performed by the investigators in the LAQV/REQUIMTE Laboratory, Department of Chemistry and Biochemistry, Faculty of Sciences, University of Porto.

The NPs tested were: 12, 40 and 60 nm diameter gold nanospheres (AuNPs) coated with citrate (15, 0.17 and 0.075 nM, respectively); ~60 nm tip-to-tip gold nanostars (AuNSs) coated with MUA (0.17 nM); ~200 nm tip-to-tip silver nanostars (AgNSs) coated with citrate (0.1 nM); 300 nm diameter selenium nanospheres (SeNPs) coated with glucose (0.1 nM). The concentrations stated above were those of the stock solutions of each NM, dilutions were used for the exposure to cells. All solutions were prepared using ultrapure water unless stated otherwise. All batches were stored at 4 ˚C.

The synthesis of AgNSs was performed via the reduction of Ag^+ with HA in an aqueous solution followed by the addition of citrate to perform a capping-reduction. A total of 9 mL of 10^{-3} mol/L of silver nitrate was added dropwise to a mix of 500 µL of 5×10^{-2} mol/L sodium hydroxide and 500 µL of 6×10^{-2} mol/L HA, under stirring. After 2 min, to the resulting aqueous solution, 100 µL of 4.13×10^{-2} mol/L (1% w/v) trisodium citrate was added and the suspension was agitated for 3 hours, after which it presented a dark grey color. This is a simple method that forgoes the use of strong surfactants (Garcia-Leis *et al.*, 2013).

To synthesize the SeNPs, glucose was used to act as the reductant and capping agent. Sodium selenite (5 mmol/L) and a glucose solution (1 mol/L) were added to get a 100 mL solution in a 250 mL Erlenmeyer flask covered at the top with tinfoil. This flask was put in an autoclave at 115 °C for 15 min. This resulted in the formation of a red suspension that

was promptly cooled. Afterward, this suspension was washed using water and centrifugated at 1000 g for 20 min a total of four times (Nie *et al.*, 2016).

For the AuNPs synthesis, the first ones to be prepared were the 12 nm diameter AuNPs. For this purpose, a stock gold (III) chloride solution was diluted to a concentration of 1 mmol/L (100 mL final volume). This solution was then transferred to a three-neck round bottom flask with a stir bar, which was equipped with a condenser and put in a hot oil bath. Under stirring, 1 mL of a 0.7 mol/L citrate aqueous solution (prepared from trisodium citrate) was quickly added to the flask. After 20-30 min under reflux, the synthesis was complete, with the suspension turning into a deep red color. This synthesis is a modification of the Frens method, which is based on the use of citrate as a reducing and stabilizing agent to get AuNPs from Au^{3+} (Zabetakis *et al.*, 2012).

For the bigger sized AuNPs (40 and 60 nm), a process similar to the 12 nm AuNPs synthesis was performed to get the seeds: 150 mL of a 2.2 mmol/L sodium citrate solution was heated in the flask previously mentioned under constant stirring at 100 ˚C, after which 1 mL of a 25 mmol/L tetrachloroauric acid ($HAuCl_4$) solution was added. The solution became a soft pink color after 10 min. Right after the synthesis of these seeds, the flask was cooled to 90 °C. To get the 40 nm AuNPs, when the desired temperature was reached, 1 mL of the $HAuCl_4$ solution was injected and, after a 30 min reaction period, the size was assessed by UV-Vis. This process was repeated until the intended size was obtained (40 or 60 nm) (Bastús *et al.*, 2011).

Finally, to produce AuNSs, an AuNPs seed solution, prepared the way described for 12 nm AuNPs, was used as a starting point. From this seed solution, 100 µL were added to 10 mL of a 0.25 mmol/L $HAuCl_4$ solution. While this solution, which had a light red/orange color, was being stirred, 100 µL of a 2 mmol/L silver nitrate solution and 50 µL of a 100 mmol/L ascorbic acid solution were added simultaneously. The solution quickly changed to a dark blue color. A wash was then performed by centrifugation at 3000 g for 15 min. The resulting pellet was resuspended in ultrapure water. The capping was then exchanged from citrate to MUA by the addition of 5 µL of a 10 mM MUA ethanolic solution. After an overnight period, the suspension was washed again as described above. (Yuan *et al.*, 2012). The aspect of the different NPs can be observed in figure 5.

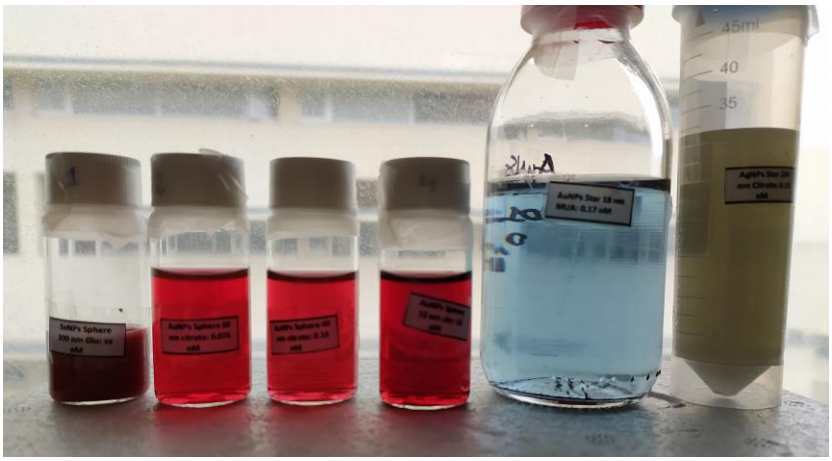

Figure 5 – Nanoparticles. From left to right: selenium nanoparticles, 60 nm gold nanoparticles, 40 nm gold nanoparticles, 12 nm gold nanoparticles, gold nanostars and silver nanostars.

For the characterization of the NPs several techniques were used, namely dynamic light scattering (DLS), electrophoretic light scattering (ELS), nanoparticle tracking analysis (NTA), ultraviolet-visible spectroscopy (UV-Vis), and transmission electron microscopy (TEM).

DLS and ELS were used for all NPs except for the 40 and 60 nm AuNPs. They were performed in a Malvern Panalytical Zetasizer Nano ZS. DLS allowed the study of the hydrodynamic size of the NPs, by assuming a spherical shape and studying the speed of the Brownian motion, which is correlated with their size (Brar and Verma, 2011). ELS enabled the study of the zeta potential. This determines the effective electric charge of an NP by measuring the difference of potential between the fluid where the NP is and the thin layer of ions of opposite charge that are attached on the NP's surface. If the NPs have a high zeta potential (positive or negative) the repulsive forces between them will be stronger and, therefore, they will be more stable and less likely to form agglomerates (Kumar and Dixit, 2017, Selvamani, 2019). The study was performed at 25 °C and each sample was read three times. Light detection was at a 17° angle, in backscatter mode, for ELS and at 273° angle for DLS (Peixoto de Almeida *et al.*, 2018).

NTA was performed using a Malvern Panalytical Nanosight NS300. This technology works similarly to DLS. It combines a digital camera detector with laser light scattering microscopy, which allows it to document single NPs. With this, not only the hydrodynamic size was studied, but also the concentration (Filipe *et al.*, 2010). This technique was applied to AuNPs (40 nm), AuNSs, AgNSs, and SeNPs.

The UV-Vis extinction spectra were obtained using a Genesys 10S UV-Vis Spectrophotometer. For AuNPs, besides the spectrum, the maximum absorbance value of the localized surface plasmon resonance (LSPR) band was recorded, as well as the absorbance at 450 nm, a part of the spectrum that is independent of the size, to be used as

a normalization. With this, values for the size and concentration were obtained for all the AuNPs tested in this work (Haiss *et al.*, 2007).

TEM micrographs were obtained for SeNPs. This was accomplished using a Jeol JEM-1400 microscope, at HEMS, I3S, University of Porto. This technique is based on the transmission electron diffraction pattern formed after the penetration of electrons through a thin layer of NPs (Egerton, 2005). The images obtained were used to assess the size of the particles, using ImageJ 1.52u software (Schneider *et al.*, 2012).

3.3 ANIMALS

Female Wistar Han rats with a bodyweight of 150-250 g were kept in sterile facilities under controlled temperature (20±2 °C), humidity (40–60%), and light (12 h-light/dark cycle) conditions, and were fed with sterile standard rat chow and tap water *ad libitum*. Isolation of hepatocytes was always conducted between 8:00 and 10:00 a.m.. This experiment was performed at the highest standards of ethics after approval by the local Ethical Committee for the Welfare of Experimental Animals (University of Porto-ORBEA) and by the national authority *Direção-Geral de Alimentação e Veterinária* (DGAV). Housing and all experimental procedures were performed by investigators accredited for laboratory animal use in accordance with the Portuguese and European legislation (law DL 113/2013, Guide for Animal Care; Directives 86/609/EEC and 2010/63/UE) under the strict supervision of veterinary physicians.

3.4 ISOLATION OF PRIMARY HEPATOCYTES

Rat anesthesia was performed by an intraperitoneal injection of a mixture of 200 µg of xylazine (Rompun® 2%, Bayer HealthCare, Germany) and 100 µg of ketamine (Clorketam® 1000, Vétoquinol, France) per 300 g body weight. Inhalation of isoflurane (IsoVet® 1000 mg/g, B. Braun VetCare, Germany) was employed during the isolation, to ensure the anesthesia was maintained.

Isolation of primary rat hepatocytes was based on a modification of the method designed by Moldeus and collaborators, which consists of an *in situ* collagenase perfusion of the liver in two steps (Moldeus *et al.*, 1978). Initially, a cannula was inserted into the portal vein and the liver was perfused with a carbonated and sterile ethylene glycol-bis(2-aminoethylether)-N,N,N′,N′-tetraacetic acid (EGTA) washing buffer, at 37 °C, for 8-10 min at a 10 mL/min flow rate. This buffer was a calcium-free balanced salt solution, with the EGTA acting as a chelating agent for that ion, decreasing the overall concentration of Ca^{2+} and irreversibly cleaving the desmosomes that bind the hepatocytes (Berry *et al.*, 1991, Puviani *et al.*, 1998). It contained 155 mL of 9 g/L glucose, 25 mL of Krebs-Henseleit (KH)

buffer at pH 7.4, which is a combination of 60 g/L sodium chloride (NaCl), 1.75 g/L potassium chloride (KCl) and 1.6 g/L potassium dihydrogen phosphate (KH_2PO_4), 25 mL of 60 g/L 4-(2-hydroxyethyl)-1-piperazineethanesulfonic acid (HEPES) (pH 8.5), 18.5 mL of minimum essential medium (MEM) non-essential amino acids solution, 18.5 mL of MEM essential amino acids solution diluted 1:5, 2.5 mL of 7 g/L glutamine and 1 mL of 47.5 g/L EGTA (pH 7.6). The inferior vena cava was immediately cut so the perfusion fluids could leave the liver. Afterward, a collagenase buffer at 37 °C was perfused through the liver until the consistency of this organ changed, which took about 8-10 min. The collagenase cleaves the collagen molecules specifically and hydrolytically and is dependent on Ca^{2+} to be activated, which does not interfere with cell adhesion at this stage due to the irreversible nature of the desmosomes' cleavage (Berry *et al.*, 1991, Puviani *et al.*, 1998). This buffer was constituted by 77.5 mL of 9 g/L glucose, 12.5 mL KH buffer (pH 7.4), 12.5 mL of 60 g/L HEPES (pH 8.5), 7.5 mL of MEM non-essential amino acids solution, 7.5 mL of MEM essential amino acids solution diluted 1:5, 2.5 mL of 19 g/L calcium chloride dihydrate ($CaCl_2 \cdot 2H_2O$), 1.25 mL of 7 g/L glutamine and 1525 U/mL of collagenase type IA from *Clostridium histolyticum*, which was only added after successful cannulation since it is expensive and should not be wasted. At this stage, the liver was extracted from the animal, by cutting the ligamentous attachments to the mesentery. The set up used in this isolation can be seen in figure 6.

Figure 6 – Hepatocyte isolation set up. Thermostatic water bath (left), peristaltic pump (center).

The liver was transferred into a petri dish that contained a suspension buffer. This buffer is composed of 124 mL of 9 g/L glucose, 20 mL KH buffer (pH 7.4), 20 mL of 60 g/L HEPES (pH 7.6), 15 mL of MEM non-essential amino acids solution, 15 mL of MEM essential amino acids solution diluted 1:5, 1.6 mL of 19 g/L $CaCl_2 \cdot 2H_2O$, 2 mL of 7 g/L glutamine, 0.8 mL of 24.6 g/L magnesium sulfate heptahydrate ($MgSO_4 \cdot 7H_2O$) and 400 mg of bovine serum albumin (to inactivate the collagenase). To help the disruption of the liver, a gentle mechanical dissociation was employed. The suspension obtained contained the hepatocytes but also other residues and types of cells, so hepatocyte purification was required. To this end, the suspension was first passed through a fine-mesh sieve and centrifuged at 50 g for three minutes at 4°C. The supernatant was rejected, and suspension buffer was added to resuspend the pellet, which contained the hepatocytes that, due to their higher density, tend to deposit. This was repeated three times or until the supernatant was clear.

Cell viability and number were assessed using a Neubauer chamber and the trypan blue method (Marquis *et al.*, 2009). This is a charged molecule that can only enter cells with damaged membranes, hence a cell with blue coloring is an indicator of its death. The number of alive and dead cells was counted, and the viability, that is the percentage of living cells, was always above 80%.

3.5 CELL PLATING AND EXPOSURE

For the cytotoxicity assay, the cells were seeded into 96-well plates at 50 x 10^3 cells per well. For metabolomics, the cells were cultured in 100 x 10 mm petri dishes at a density of 6×10^6 cells per dish. The hepatocytes were cultured in William's Medium E medium supplemented with 10 % heat-inactivated fetal bovine serum, 10 μg/mL gentamicin, 2 ng/mL insulin from bovine pancreas, 5 nM of dexamethasone, and a combination of penicillin G and streptomycin at 100 U/mL and 100 μg/mL, respectively. The plates used for cell seeding were previously coated with collagen G (Biochrom Ltd.) diluted in Hanks balanced salt solution (HBSS, without calcium and magnesium) to a final concentration of 40 ng/mL. The hepatocytes were incubated overnight at 37 °C so they could adhere to the bottom of the plates.

Then, on the day of the cytotoxicity experiment, the cell culture medium in each well was replaced by each test NPs (12, 40, and 60 nm AuNPs, 60 nm AuSNs and 200 nm AuSNs), diluted 10x from the stock, in the culture medium. For the SeNPs, 20x, 30x, 40x, 50x, 60x, 70x, 80x and 90x dilutions were also studied.

3.6 CYTOTOXIC ASSAYS

The 3-(4,5-dimethylthiazol-2-yl)-2,5-diphenyltetrazolium bromide (MTT) test is a metabolic activity assay based on the cellular reduction by dehydrogenases (mainly mitochondrial but also cytoplasmatic) of tetrazolium salts to colored formazan products. MTT is a soluble, positively charged yellow dye that enters the cells easily, and is converted to formazan, forming insoluble purple precipitates. These need to be solubilized to enable the absorbance reading, which is proportional to the amount of formazan formed (Ciappellano *et al.*, 2016, Martin and Sarkar, 2019). After the exposure period to NPs, the culture medium was removed and the cells were incubated with 1 mg/mL of MTT solution for 30 min at 37 °C, with 5% CO_2. The resulting precipitates were dissolved with dimethyl sulfoxide and the absorbance was read at 550 nm in a multi-well plate reader BioTek Synergy™ HT (BioTek Instruments, Inc.).

The neutral red (NR) dye uptake technique was also used to assess cell viability. This is an uncharged compound that is protonated and retained inside acidic lysosomes of live cells and, since energy is needed to maintain the pH gradients, reduced dye detection will correlate to reduced cell viability (Ciappellano *et al.*, 2016, Martin and Sarkar, 2019). After the exposure period to NPs, the culture medium was removed and the cells were incubated with 50 μg/mL of NR for 50 min at 37 °C, with 5% CO_2. After that, the cells were washed with HBSS to remove the non-incorporated dye, and a lysis solution (50% ethanol, 49% distilled water, 1% glacial acetic acid) was used to dissolve the dye. The absorbance was read at 540 nm.

Negative (only culture medium) and positive controls (1% Triton X-100) were included in both assays. Data were expressed as % of MTT reduction and % of NR incorporation normalized to negative and positive controls.

3.7 METABOLOMICS

3.7.1 COLLECTION OF SAMPLES

For metabolomics, the cells were cultured in petri dishes at a density of 6×10^6 cells per petri dish and exposure was performed as explained above. After 24 h of exposure, samples for the study of intracellular metabolome were extracted. Six independent experiments were performed, giving a total of 42 samples for metabolomic analysis. All tubes referred below were coated with a solution of methanol:water (80:20 v/v) and all the procedure was performed on ice.

Firstly, the culture medium was removed. Then, the petri dishes were washed twice with 12 mL of sodium chloride (0.9 %), to remove interferences. Afterward, 9 mL of the ice-cold methanol:water solution was added to quench the metabolites, and the cells were

scraped from the bottom and transferred to a falcon. The cells were sonicated on ice for 30 seconds, centrifuged at 3000 g for 10 min at 4 °C and the supernatant was transferred to new falcons.

Quality controls (QCs) were prepared by combining an equal volume of all samples (controls and exposures) into a glass vial. These were used to assess the reproducibility of the metabolomic results, as well as for the identification of metabolites. All the samples and QCs were stored at -80 °C until needed.

3.7.2 DERIVATIZATION OF ANALYTES

To obtain the spectra of the endometabolome, the method used was based on protocols from our groups (Lima *et al.*, 2018, Lima *et al.*, 2020). To be able to analyze all components of the metabolome, derivatization was performed to increase the volatilization of the metabolites. In a glass vial, 1 mL of each sample was added, followed by 8 µL of desmosterol (1 mg/mL), which is the internal standard. The mixture was vortexed and was let to evaporate at room temperature with a flow of nitrogen gas. When this was achieved, 100 µL of N-methyl-N-(trimethylsilyl) trifluoroacetamide (for derivatization) was added to the vial, vortexed, and incubated for 30 min at 80 °C to perform the derivatization. When the time ended, the mixture was transferred to autosampler vials and taken to the GC-MS system.

3.7.3 GC-MS ANALYSIS

For this study, the equipment used was an EVOQ-436 gas chromatography coupled with a Bruker Triple Quadrupole mass detector and a Bruker MS workstation software version 8.2. The analysis was performed using a Rxi-5Sil MS (30 m × 0.25 mm × 0.25 µm) column (Restek), and using helium C-60 (Gasin, Portugal) with a flow of 1 mL/min as a carrier gas, in full scan mode. A volume of 2 µL of each sample was injected, in a split mode (1/10 ratio), using a CombiPAL automatic autosampler (Bruker), with the injecting port heated to 250 °C. The oven temperature was 70 °C for 2 min, followed by an increase to 250 °C at a rate of 15 °C/min, which was held for 2 min. Then, the temperature was increased to 300 °C at a rate of 10 °C/min and kept there for 8 min, for a total of 26 min per sample. The manifold temperature was 40 °C and the transfer line temperature was 250 °C. The mass spectra were obtained by the electron impact mode and the mass range was from 40-600 *m/z*. The emission current was 50 µA and the electron multiplier was set in a relative mode to an autotune procedure.

The samples were injected randomly, and a QC was injected every 5 samples to ensure reproducibility, with a total of 42 samples and 9 QCs.

3.7.4 GC-MS DATA PRE-PROCESSING

The identification of metabolites was performed using reference standards. In the cases where this was not possible, the National Institute of Standards and Technology (NIST 14) spectral library database and a comparison of the theoretical and experimental Kovats index were combined to obtain an identification.

The chromatograms obtained from GC-MS were pre-processed using MZmine 2.53 for chromatogram deconvolution, peak detection, alignment, and baseline correction (Pluskal *et al.*, 2010). Parameters that were used to perform this pre-process included *m/z* range (50-500) and *m/z* tolerance (0.2), MS data noise level (1×10^5), retention time (RT) range (4.40-23.00), peak duration range (0.02-0.5), and chromatogram baseline level (1×10^4). The ions (*m/z)* with values of relative standard deviation (RSD) higher than 30% as well as artifact ions were excluded. The remainder values were normalized to the total area of the chromatogram and a process of variable selection was performed to refine the matrix and remove data from uncontrolled confounding factors. This was done by calculating the *p*-value for each *m/z* RT pair using Metaboanalyst and all values with $p > 0.05$ were removed.

3.8 STATISTICAL ANALYSIS

The statistical analysis for the MTT and NR assays was performed using GraphPad Prism 8 software (GraphPad Software, San Diego, CA). The normality of the data was assessed through the Anderson-Darling, D'Agostino & Pearson, Shapiro-Wilk, and Kolmogorov-Smirnov tests. All obtained results had a non-normal distribution and, so, statistical comparison of the groups with the control was performed with a one-way analysis of variance on ranks, also known as the Kruskal-Wallis test. All the results obtained are expressed as the mean ± standard error of the mean and the values were considered statistically significant when $p < 0.05$.

Multivariate analysis to compare the metabolomic results of the NPs with the controls was conducted through principal component analysis (PCA), for the QCs, and partial least squares discriminant analysis (PLS-DA) with a Pareto scaling, for the treatments, using the SIMCA-P software. The models obtained were validated using a permutation test of 200 permutations of two components and Y-observations. Afterward, the metabolites that were involved in the discrimination of the control cells *vs*. the NP exposed cells were identified through the values of variable importance of projection (VIP) from the PLS-DA, which had to be higher than 1 for that metabolite to be considered potentially discriminant. For confirmation, three univariate analyses were implemented. Since all results followed a non-normal distribution, the non-parametric unpaired Mann-Whitney test was used to obtain the *p*-values, with the GraphPad Prism 8 software (GraphPad Software, San Diego, CA), the

effect size (and standard error associated) and percentage of variation (and uncertainty of the percentage of variation) were also obtained. For the metabolites to be discriminant, the *p*-value had to be inferior to 0.05, the effect size higher than the standard error, and the percentage of variation higher than the uncertainty of the percentage of variation (Berben *et al.*, 2012). The metabolites upregulated had positive values of effect size and percentage of variation, while the metabolites downregulated had negative values of effect size and percentage of variation. Finally, a pathway analysis was performed with MetaboAnalyst 3.0 (Pang *et al.*, 2020) to assess the metabolic pathways altered in each NP related to each metabolite and the significance of that pathway. Only the ones with a p-value ≤ 0.05 were considered.

4. RESULTS

4.1 CHARACTERIZATION OF NANOPARTICLES

The NPs were synthesized and characterized as described above. The results from the different techniques used for the characterization of NPs can be seen in table 1.

Table 1 – Characterization of the NPs.

NPs	AuNPs (12 nm)	AuNPs (40 nm)	AuNPs (60 nm)	AuNSs (60 nm)	AgNSs (200 nm)	SeNPs (300 nm)
UV-Vis Diameter (nm)	12	40	59	n.a.	n.a.	n.a.
DLS Hydrodynamic diameter (nm)	15.7 ± 0.1	n.d.	n.d.	67.9 ± 0.4	136.8 ± 1.5	378.0 ± 4.1
NTA Hydrodynamic diameter (nm)	n.a.	54.4 ± 1.9	n.d.	62.0 ± 0.7	190.4 ± 4.4	196.6 ± 3.8
TEM Diameter of tip-to-tip (nm)	n.d.	n.d.	n.d.	n.d.	n.d.	328.8 ± 18.8
UV-Vis Concentration (nM)	15	0.17	0.075	n.a.	n.a.	n.a.
NTA Concentration (nM)	n.a.	n.d.	n.d.	0.17	0.10	0.10
ELS Zeta potential (mV)	-49.0 ± 5.1	n.d.	n.d.	-33.8 ± 0.6	-38.3 ± 0.6	-42.9 ± 0.3

Abbreviations: AgNSs (silver nanostars); AuNPs (gold nanospheres); AuNSs (gold nanostars); DLS (dynamic light scattering); ELS (electrophoretic light scattering); SeNPs (selenium nanospheres); n.a. (non-applicable); n.d. (not determined); NPs (nanoparticles); NTA (nanoparticle tracking analysis); TEM (transmission electron microscopy); UV-Vis (ultraviolet-visible spectroscopy). All these data were kindly provided by the investigators of the LAQV/REQUIMTE Laboratory, Department of Chemistry and Biochemistry, Faculty of Sciences, University of Porto.

All the NPs (except 40 and 60 nm AuNPs) have a negative charge, as demonstrated by their zeta potential, due to the capping (citrate, MUA, and glucose) used. Different results were obtained with the different techniques for the size of the NPs as the different techniques analyze different parameters, namely hydrodynamic size (NTA) and tip to tip size (TEM).

The UV-Vis spectrum was obtained for all the NPs, and they are represented in figure 7.

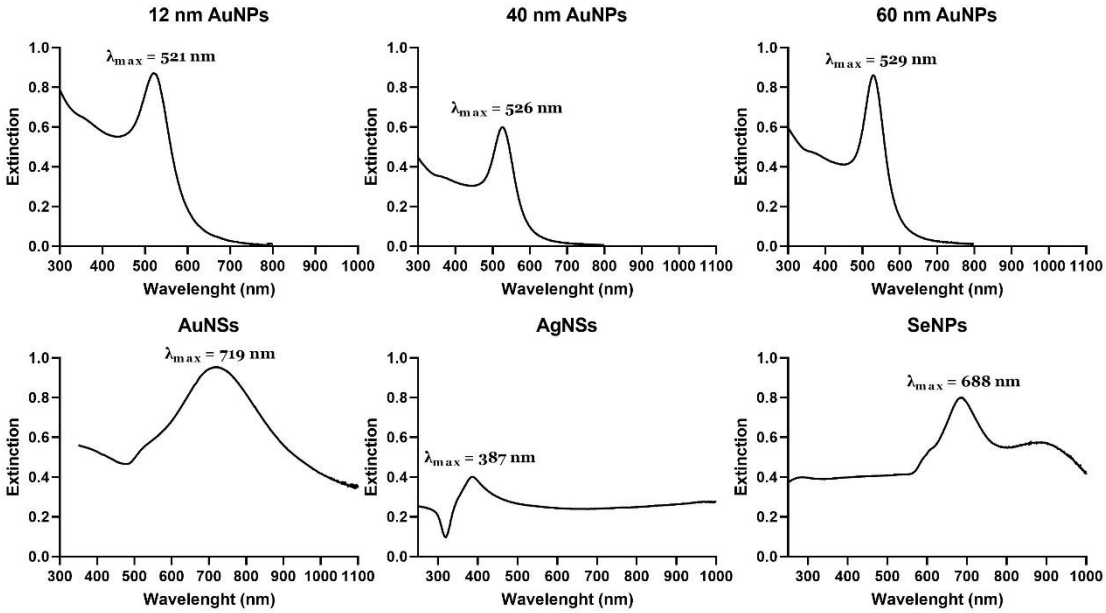

Figure 7 – UV-Vis spectrum of the nanoparticles and maximum extinction wavelength.

The images obtained from TEM can be seen in figure 8.

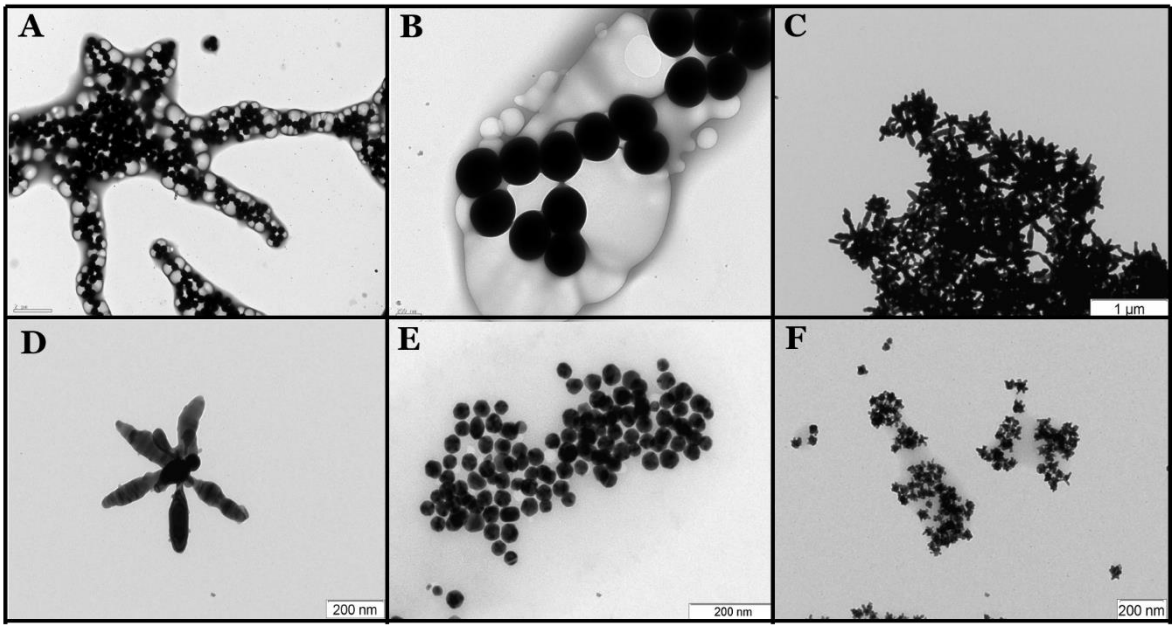

Figure 8 – TEM images of nanoparticles. SeNPs (A, B), AgNSs (C, D), AuNPs (E) and AuNSs (F). C, D, E and F are representative. All images were provided by the investigators of the LAQV/REQUIMTE Laboratory, Department of Chemistry and Biochemistry, Faculty of Sciences, University of Porto.

4.2 CYTOTOXICITY

The cell viability of the primary hepatocytes after 24 h exposure to the NPs was evaluated by the MTT and NR assays. Figures 9 and 10 show the results obtained for AuNPs/AuNSs/AgNSs and SeNPs, respectively. The concentrations of SeNPs are dilutions from the stock solution.

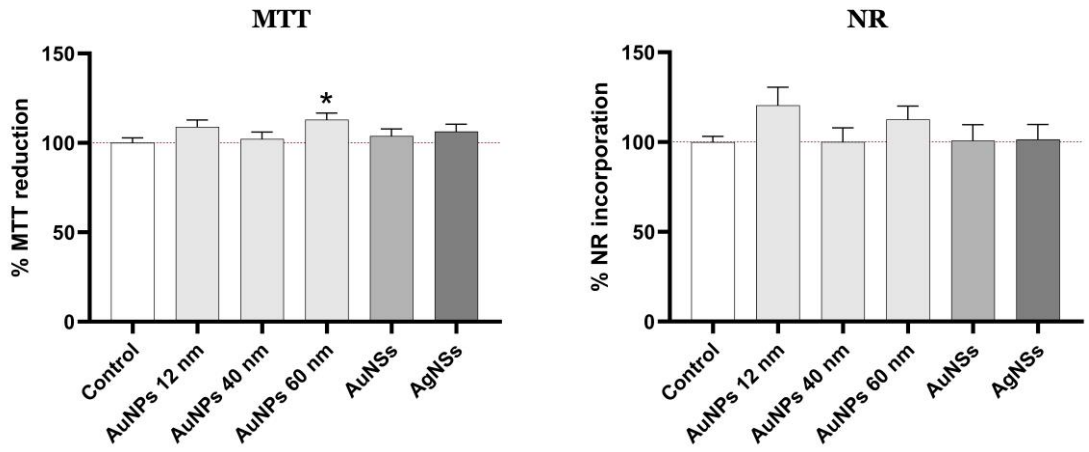

Figure 9 – Percentage of MTT reduction (left) and percentage of NR incorporation (right) for 12 nm AuNPs (1.50 nM), 40 nm AuNPs (0.017 nM), 60 nm AuNPs (7.5×10^{-4} nM), AuNSs (0.017 nM) and AgNSs (0.010 nM). Comparison with controls performed with one-way ANOVA Kruskal-Wallis test. *p ≤ 0.05.

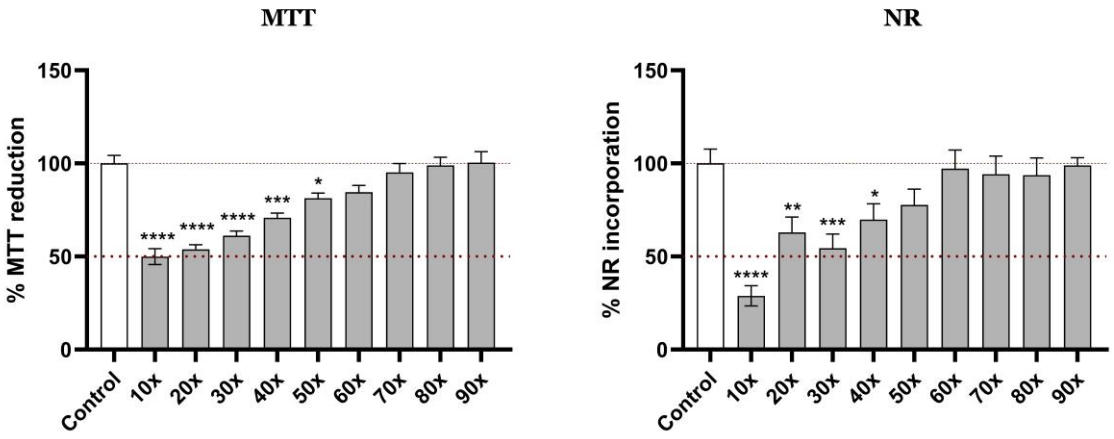

Figure 10 – Percentage of MTT reduction (left) and percentage of NR incorporation (right) for SeNPs Concentrations: 10x (0.010 nM), 20x (5.0×10^{-3} nM), 30x (3.33×10^{-3} nM), 40x (2.5×10^{-3} nM), 50x (2.0×10^{-3} nM), 60x (1.67×10^{-3} nM), 70x (1.43×10^{-3} nM), 80x (1.25×10^{-3} nM) and 90x (1.11×10^{-3} nM). Comparison with controls performed with one-way ANOVA Kruskal-Wallis test. *p ≤ 0.05, **p ≤ 0.01, ***p ≤ 0.001 and ****p ≤ 0.0001.

All the AuNPs, the AuNSs, and the AgNSs had no cytotoxicity at the concentrations tested in both the MTT and NR assay after 24 h. The 60 nm AuNPs had a significant increase in the percentage of MTT reduction ($p < 0.05$). Hence, a 10x dilution of the stock solutions

was used for the metabolomics study, which is 1.50 nM of 12 nm AuNPs, 0.017 nM of 40 nm AuNPs, 7.5×10^{-4} nM of 60 nm AuNPs, 0.017 nM of AuNSs, and 0.010 nM of AgNSs.

For the SeNPs, several concentrations were tested. In the MTT assay, concentrations of 0.010 nM ($p < 0.0001$), 5.0×10^{-3} nM ($p < 0.0001$), 3.33×10^{-3} nM ($p < 0.0001$), 2.5×10^{-3} nM ($p < 0.001$) and 2.0×10^{-3} nM ($p < 0.05$) (10x, 20x, 30x, 40x and 50x dilutions of the stock solution, respectively) elicited a significative decrease of cell viability after 24 h of exposure. In the NR assay, exposure of the cells to concentrations of 0.010 nM ($p < 0.0001$), 5.0×10^{-3} nM ($p < 0.01$), 3.33×10^{-3} nM ($p < 0.001$) and 2.5×10^{-3} nM ($p < 0.05$) (10x, 20x, 30x and 40x dilutions of the stock solution, respectively) led to a significative decrease in cell viability. Both assays showed that SeNPs have a concentration-dependent toxicity to primary hepatocytes, but the MTT assay was more sensitive to these changes. Based on this, a concentration of 1.67×10^{-3} nM was chosen for the metabolomic study, as it was the highest concentration that did not induce significative cytotoxicity in both tests. The IC50 of the SeNPs obtained in the MTT assay was of 0.010 nM.

4.3 METABOLOMICS RESULTS

A total of 167 chromatographic peaks were detected and analyzed from the GC-MS chromatograms. After this, two multivariate analyzes (PCA and PLS-DA) were performed with the results obtained. The PCA performed with the QCs can be seen in figure 11, where they can be seen all pooled together. This proves the reproducibility of the results since the QCs were all obtained from the same original sample and, therefore, should be similar. The PLS-DA analysis to compare the controls to each of the NPs tested can be seen in figure 12. One of the replicas related to the SeNPs was excluded from the respective PLS-DA since it presented a value outside the range of all other results.

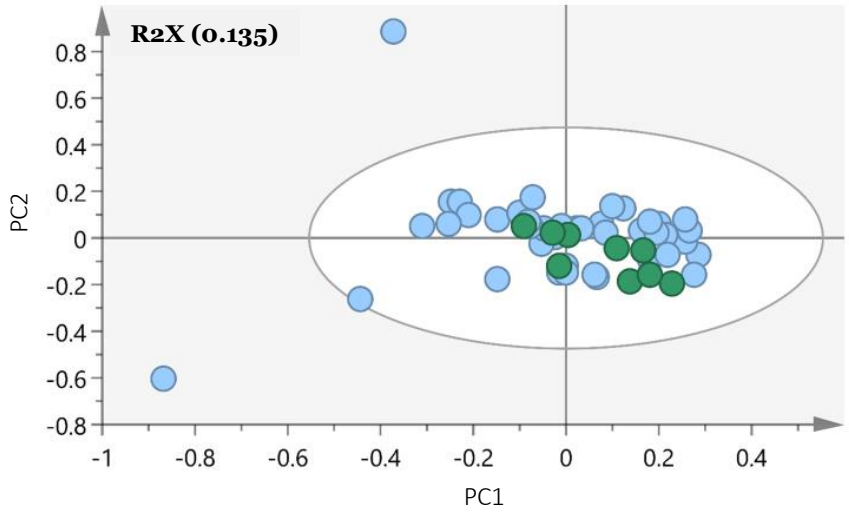

Figure 11 – PCA of QCs (green) and samples (light blue). The QCs represent a pool of all samples, controls and treatments, and are identical, which should lead to equal samples. Since they are all together, the reproducibility was confirmed.

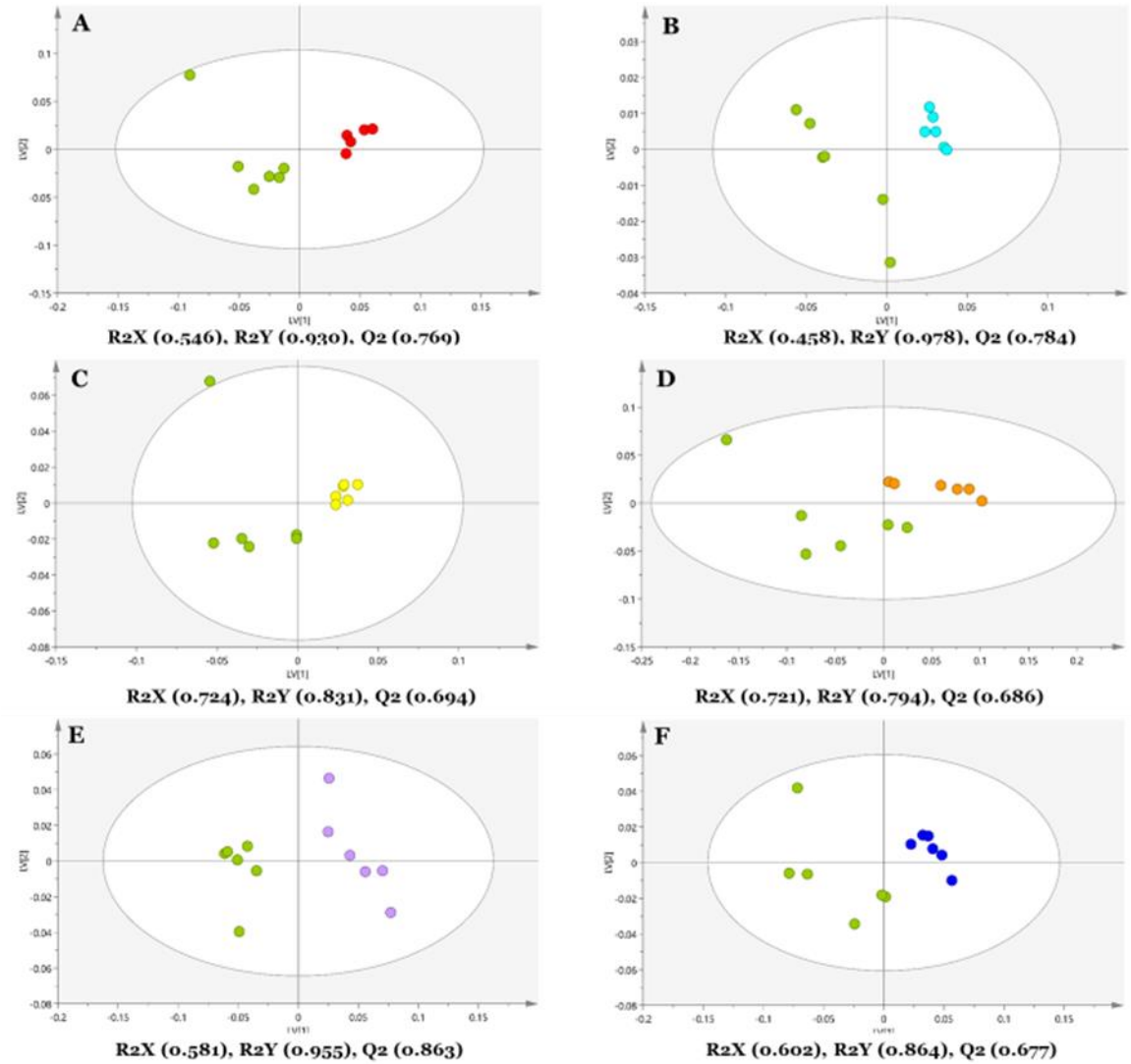

Figure 12 – PLS-DA models. A – Control (green) *vs.* 24 h exposure to 1.67×10^{-3} nM SeNPs (red); B – control (green) *vs.* 24 h exposure to 1.50 nM 12 nm AuNPs (light blue); C – control (green) *vs.* 24 h exposure to 0.017 nM 40 nm AuNPs (yellow); D – control (green) *vs.* 24 h exposure to 0.017 nM AuNSs (purple); F – control (green) *vs.* 24 h exposure to 0.010 nM AgNSs (dark blue). Q2 superior to 0.5 indicates a discrimination between control and NP exposure samples.

All the models showed differences between the control groups and the NP exposed cells, with values of Q2, that assess the predictive capability of the model, all above the limit of 0.5 necessary for discrimination. All the models were valid, as can be seen in the permutation tests (figure 13), which assess the overfitting of the models, that is, if the model fits the results used but has low prediction power. This is done by comparing the original R2 and Q2 of the PLS-DA (far right) with those obtained by 200 permutations in which the order of the Y-observations (classes) was switched randomly. Our PLS-DA models passed validation because all Q2 and R2 values are lower than the original and the regression line of the Q2-values intersects the x-axis at or below zero.

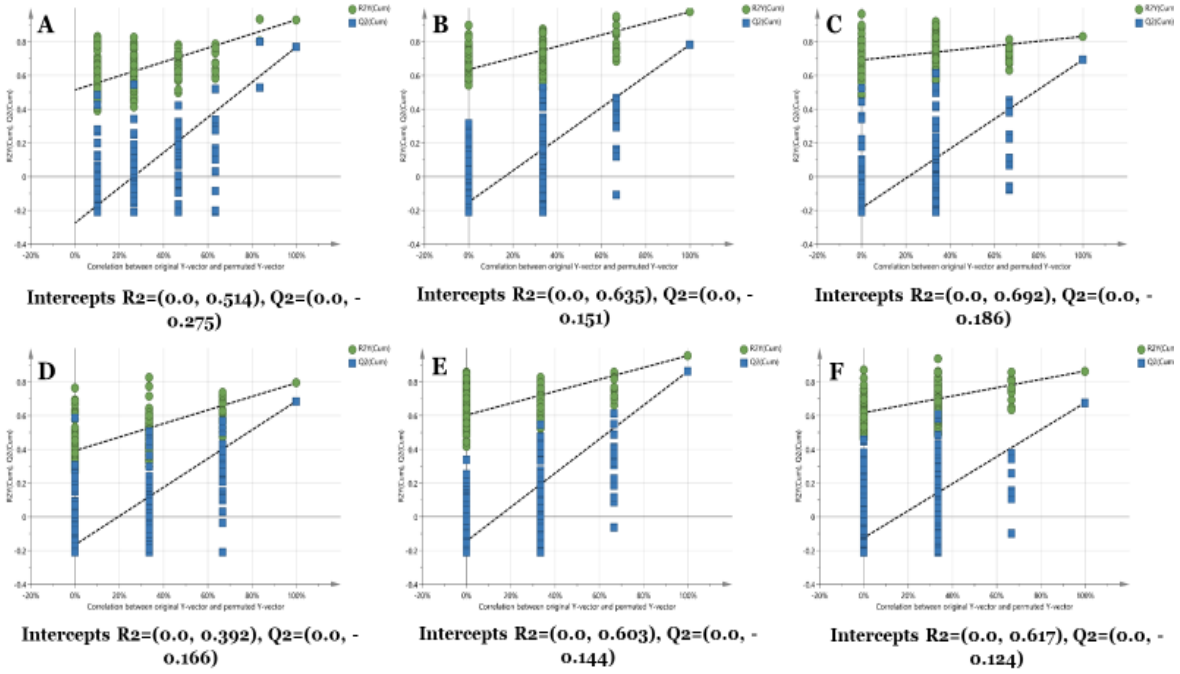

Figure 13 – Validation of PLS-DA models through permutation tests (200 permutations, two components). A – 24 h exposure to 1.67×10^{-3} nM SeNPs; B – 24 h exposure to 1.50 nM 12 nm AuNPs; C – 24 h exposure to 0.017 nM 40 nm AuNPs; D – 24 h exposure to 7.5×10^{-4} nM 60 nm AuNPs; E – 24 h exposure to 0.017 nM AuNSs; F - 24 h exposure to 0.010 nM AgNSs. Validation required Q2 (blue) and R2 (green) values lower than original (far right) and intersection of regression line of Q2 values (blue) with x-axis at or below zero.

The discriminant metabolites that cause the separation between the controls and the hepatocytes exposed to the different NPs were obtained and compiled in table 2. For this, the metabolites with VIPs (importance) superior to 1 were statistically analyzed, which also allowed us to understand if they were increased or decreased (table 3). The boxplots of the metabolites are presented in figures 14-19. A total of 5 metabolites were significantly altered in SeNPs, were 2 were classified as unknown. In 12 nm AuNPs, 8 metabolites were identified, with 3 unknowns. In 40 nm AuNPs, 6 metabolites were identified, with 2 classified as unknowns. In 60 nm AuNPs, 7 metabolites were identified, with 3 unknowns. In AuNSs, 4 metabolites were identified, with one unknown. Lastly, in AgNSs, 4 metabolites were identified, with 1 unknown.

Table 2 – List of discriminant metabolites for all NPs.

Name	RT	m/z	Literature kovat	Calculate kovat	Match	Rmatch	CAS	HMDB
Unknown 1	4.603	207;208;133;209;105;73;191;135;75;103	–	1013	–	–	–	–
Unknown 2	4.636	146;73;238;119;59;147;77;75;239;148	–	1015	–	–	–	–
1,3-Propanediol, 2TMS derivate	5.117	147;130;115;73;148;177;149;131;66;133	1051	1057	937	937	504-63-2	–
Unknown 3	5.449	73;311;207;223;89;193;191;312;59;133	–	1086	–	–	–	–
L-Alanine, 2TMS derivative	5.672	116;73;147;117;190;118;74;75;59	1095	1105	731	780	56-41-7	HMDB0000161
Unknown 4	5.765	73;155;225;240;88;105;110;278;133;221	–	1113	–	–	–	–
2-Hydroxybutyric acid, 2TMS derivate	6.616	73;131;147;75;74;66;132;148;133	1136	1189	709	762	3347-90-8	HMDB0000008
Unknown 5	6.693	147;73;148;149;66;190;131;74;72;219	–	1195	–	–	–	–
Unknown 6	7.158	154;73;110;117;75;77;59;69;56	–	1241	–	–	–	–
L-Serine, 2TMS derivate	7.308	116;132;73;75;147;103;57;144;133	1252	1255	708	765	56-45-1	HMDB0000187
L-Aspartic acid, 2TMS derivate	8.850	73;160;130;75;117;116;147;74;161	1420	1418	877	885	56-84-8	HMDB0000191
Aminomalonic acid, tris(trimethylsilyl)	9.236	73;147;218;320;174;219;86;148;133	1485	1463	676	763	1068-84-4	HMDB0001147
L-Threonic acid, tris(trimethylsilyl) ether, trimethylsilyl ester	9.945	73;147;292;205;220;117;103;217;293; 148	1523	1548	652	722	7306-96-9	HMDB0000943

Name	RT	m/z	Literature kovat	Calculate kovat	Match	Rmatch	CAS	HMDB
L-Glutamine, N,N'di(trifluoroacetyl)-. Trimethylsilyl esther	10.030	73;116;75;212;77;152;69;55;74	1513	1558	529	593	56-85-9	HMDB0000641
Unknown 7	10.308	73;211;75;133;283;227;212;59;239;129	–	1592	–	–	–	–
L-(-)-Sorbofuranose, pentakis(trimethylsilyl) ether	11.788	73;217;147;218;75;103;129;74;219	1779	1789	666	773	36468-68-5	–
D-Galactose, 5TMS derivative	12.516	73;204;191;147;217;205;75;129;206;74	1970	1995	698	809	3646-73-9	HMDB0000143
D-Glucopyranose, 5TMS derivative	12.958	204;73;191;147;205;217;206;189;129; 192	2037	2061	904	906		–
2-Palmitoylglycerol, 2TMS derivative	17.434	73;129;218;103;147;57;75;55	2558	2643	750	811	23470-00-0	HMDB0011533
Docosahexaenoic acid, TMS derivative	17.469	73;79;91;117;75;67;93;105;119;106	2562	2647	883	884	6217-54-5	HMDB0002183
Unknown 8	20.235	73;57;79;55;93;117;58;69;103;80	–	2979	–	–	–	–
Cholesterol, TMS derivative	22.305	129;73;329;368;75;57;95;55;81	3150	3244	912	912	57-88-5	HMDB0000067

Abbreviations: RT (retention time); *m/z* (identifiable ions); Kovat (index, characteristic of each metabolite); CAS (Chemical Abstracts Service registry number, unique for each chemical compound); HMDB (human metabolome database number, characteristic of human metabolites). Similar literature and calculated kovats (less than a difference of 50), combined with a match and Rmatch values superior to 700 indicate good identification of the metabolites.

Table 3 – List of discriminant metabolites with p-value, percentage of variation, and effect size.

300 nm SeNPs

Metabolite	**↓ L-serine**	**↓ L-aspartic acid**	**↑ D-Galactose**	**↑ Unknown 2**	**↓ Unknown 5**
***p* value**	0.0303	0.0173	0.0173	0.0173	0.0303
% variation ± uncertainty	-47.731 ± 19.303	-14.905 ± 5.019	53.819 ± 16.978	110.250±27.698	-35.281 ± 16.294
ES ± ES_{SE}	1.619± 1.279	-1.734 ± 1.305	1.302± 1.214	1.444± 1.242	-1.395± 1.232

12 nm AuNPs

Metabolite	**↑ 1,3-Propanediol**	**↓ 2-Hydroxybutyric acid**	**↓ L-Threonic acid**	**↓ D-Glucopyranose**	**↓ Docosahexaenoic acid**	**↑ Unknown 1**	**↑ Unknown 3**	**↓ Unknown 7**
***p* value**	0.0260	0.0260	0.0022	0.0260	0.0152	0.0260	0.0043	0.0260
% variation ± uncertainty	86.344± 23.927	-32.097 ± 14.064	-59.695 ± 16.874	-49.001 ± 16.525	-47.601 ± 19.623	115.109 ± 26.355	223.173 ± 18.388	-71.361 ± 42.487
ES ± ES_{SE}	1.343± 1.175	-1.449± 1.195	-2.688± 1.499	-2.093 ± 1.339	-1.697 ± 1.246	1.477± 1.200	3.057± 1.608	-1.392± 1.184

40 nm AuNPs

Metabolite	**↓ 2-Hydroxybutyric acid**	**↓ L-Threonic acid**	**↓ D-Glucopyranose**	**↓ L-(-)-Sorbofuranose**	**↑ Unknown 3**	**↑ Unknown 4**
***p* value**	0.0043	0.0022	0.0411	0.0152	0.0022	0.0152
% variation ± uncertainty	-32.529 ± 8.705	-57.390 ± 15.473	-41.804 ± 20.315	-43.710 ± 19.911	260.731 ± 16.731	135.955 ± 27.299
ES ± ES_{SE}	-2.536± 1.456	-2.772± 1.524	-1.387± 1.183	-1.497± 1.204	3.605± 1.781	1.580± 1.221

60 nm AuNPs

Metabolite	↓ 2-Hydroxybutyric acid	↓ Aminomalonic acid	↓ 2-Palmitoylglycerol	↓ Cholesterol	↑ Unknown 3	↑ Unknown 4	↑ Unknown 6
***p* value**	0.0022	0.0411	0.0152	0.0043	0.0022	0.0173	0.0411
% variation ± uncertainty	-32.986 ± 8.299	-27.112 ± 11.343	-60.356 ± 33.540	-41.587 ± 11.474	278.227± 14.935	138.509± 27.200	-38.380± 17.942
ES ± ES_{SE}	-2.536± 1.456	-1.474± 1.199	-1.374± 1.180	-2.439± 1.429	4.152± 1.962	1.603± 1.226	-1.411± 1.187

60 nm AuNSs

Metabolite	↓ 2-Hydroxybutyric acid	↑ L-alanine	↓ Cholesterol	↓ Unknown 3
***p* value**	0.0087	0.0260	0.0260	0.0152
% variation ± uncertainty	-36.950 ± 10.612	77.407 ± 16.211	-38.801 ± 18.303	-56.682 ± 25.168
ES ± ES_{SE}	-2.276± 1.386	1.835± 1.277	-1.402± 1.186	-1.675± 1.241

200 nm AgNSs

Metabolite	↓ Aminomalonic acid	↓ L-Glutamine	↓ Cholesterol	↓ Unknown 8
***p* value**	0.0260	0.0260	0.0260	0.0152
% variation ± uncertainty	-29.823 ± 11.913	-26.710 ± 11.340	-37.237 ± 20.334	-62.934 ± 29.339
ES ± ES_{SE}	-1.568± 1.218	-1.449± 1.195	-1.199± 1.149	-1.668± 1.240

Abbreviations: ES (effect size); ES_{SE} (effect size standard deviation). Metabolites increased related to positive variation and effect size, decreased metabolites related to negative variation and effect size. Variation and effect size had to be higher than their respective uncertainty/error to be considered significative, as well as have a *p*-value below 0.05.

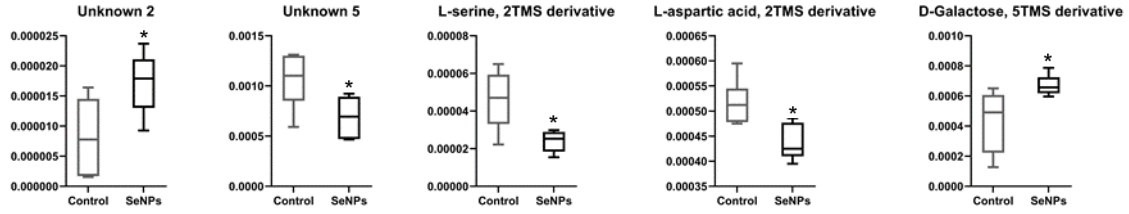

Figure 14 – Boxplots of altered metabolites after 24 h exposure of cells to 1.67×10^{-3} nM of SeNPs. * $p<0.05$.

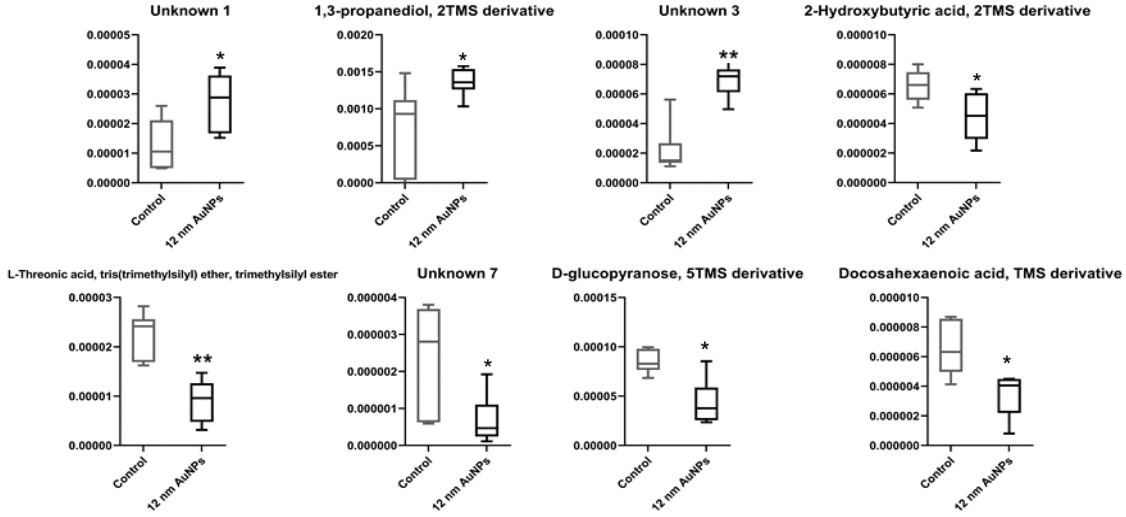

Figure 15 – Boxplots of altered metabolites after 24 h exposure of cells to 1.50 nM of 12 nm AuNPs. * $p<0.05$, ** $p<0.01$.

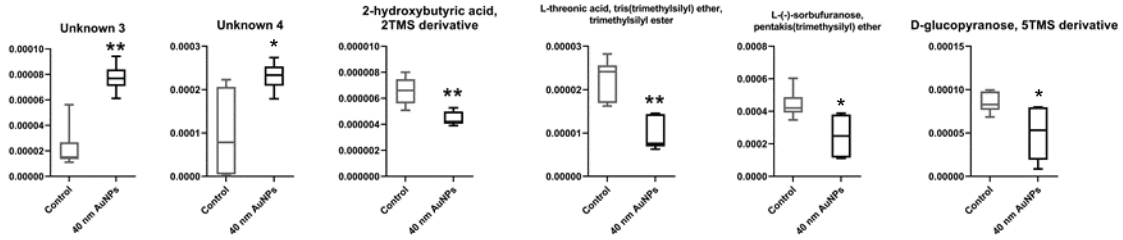

Figure 16 – Boxplots of altered metabolites after 24 h exposure of cells to 0. 017 nM of 40 nm AuNPs. * $p<0.05$, ** $p<0.01$.

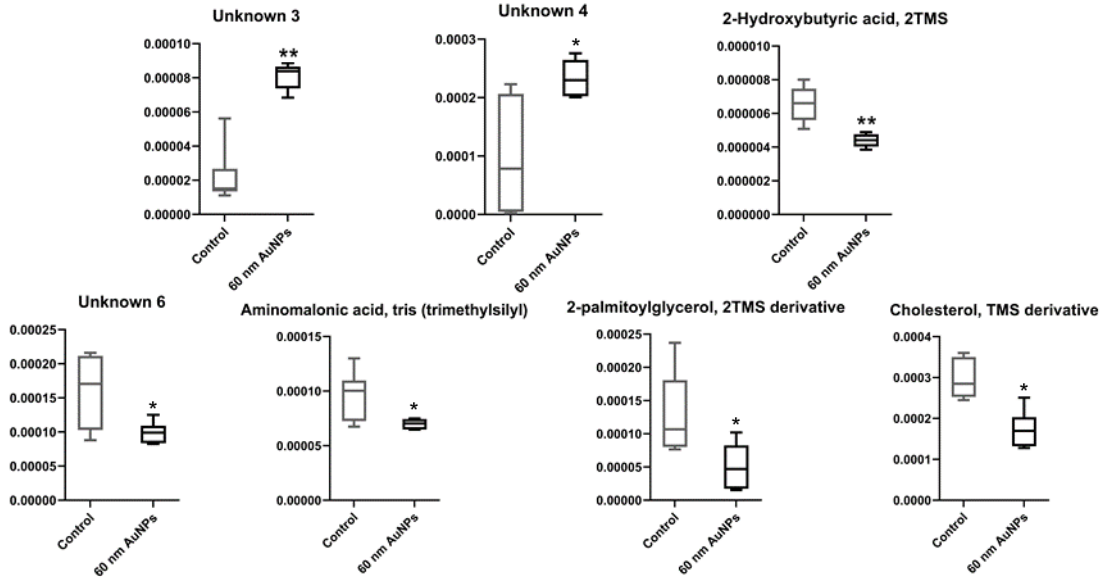

Figure 17 – Boxplots of altered metabolites after 24 h exposure of cells to 7.5×10^{-4} of 60 nm AuNPs. * $p<0.05$, ** $p<0.01$.

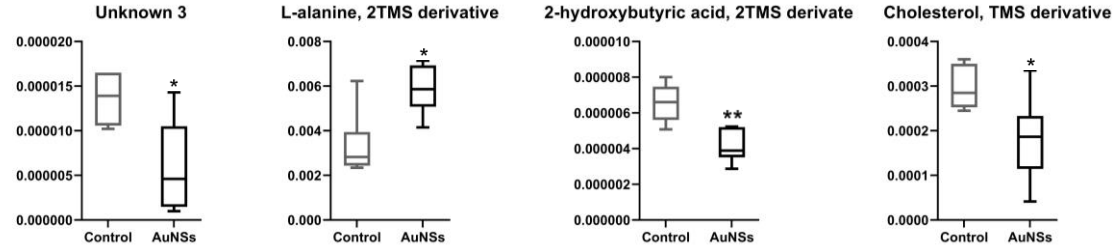

Figure 18 – Boxplots of altered metabolites after 24 h exposure of cells to 0.017 nM of AuNSs. * p<0.05, ** p<0.01.

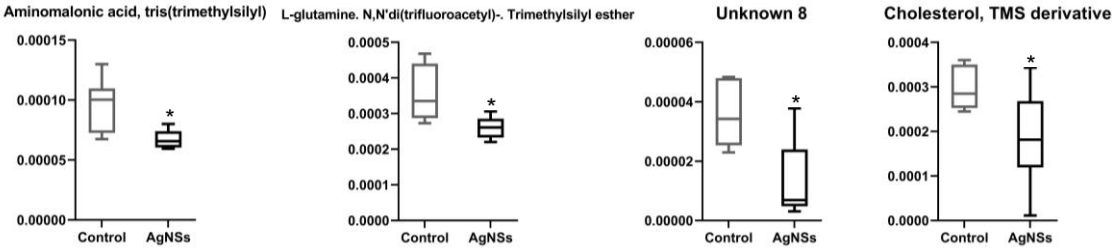

Figure 19 – Boxplots of altered metabolites after 24 h exposure of cells to 0.010 nM of AgNSs. * p<0.05.

Cells exposed to SeNPs had higher levels of D-galactose and lower levels of L-aspartic acid and L-serine. Cells exposed to 12 nm AuNPs had higher levels of 1,3-propanediol and lower levels of 2-hydroxybutyric acid, L-threonic acid, D-glucopyranose, and docosahexaenoic acid. Cells exposed to 40 nm AuNPs had lower levels of 2-hydroxybutyric acid, L-threonic acid, D-glucopyranose, and L-(-)-sorbofuranose. Cells exposed to 60 nm AuNPs had lower levels of 2-hydroxybutyric acid, aminomalonic acid, 2-palmitoyilglycerol, and cholesterol. Cells exposed to AuNSs had higher levels of L-alanine and lower levels of 2-hydroxybutyric acid and cholesterol. Lastly, cells exposed to AgNSs had lower levels of aminomalonic acid, L-glutamine, and cholesterol. All gold nanoparticles led to a downregulation of 2-hydroxybutyric acid. All these differences are statistically significant as compared with the controls.

A total of 13 metabolic pathways were significantly altered ($p \leq 0.05$) amongst all the NPs, as obtained from MetaboAnalyst (figures 20-23). Only one pathway was obtained altered after exposure of cells to 12 and 40 nm AuNPs.

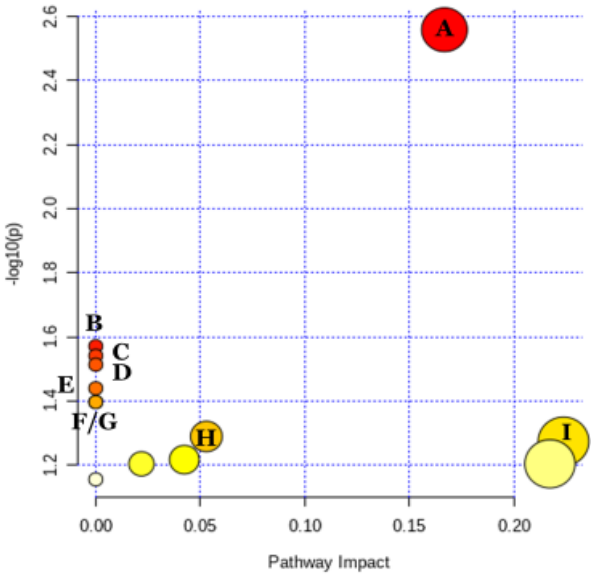

Figure 20 – Metabolic pathways significantly altered in cells exposed to 1.67×10-3 nM of SeNPs for 24 h. A- aminoacyl-tRNA biosynthesis (L-aspartic acid, L-serine. p=0.002763); B- Arginine biosynthesis (L-aspartic acid, p= 0.02687); C- Nicotinate and nicotinamide metabolism (L-aspartic acid, p= 0.028771); D- Histidine metabolism (L-aspartic acid, p= 0.030669); E- Pantothenate and CoA biosynthesis (L-aspartic acid, p= 0.036348); F- beta-Alanine metabolism (L-aspartic acid, p= 0.040123); G- Sphingolipid metabolism (L-serine, p= 0.040123); H -Galactose metabolism (D-galactose, p= 0.051386); I- Alanine, aspartate and glutamate metabolism (L-aspartic acid, p= 0.053254).

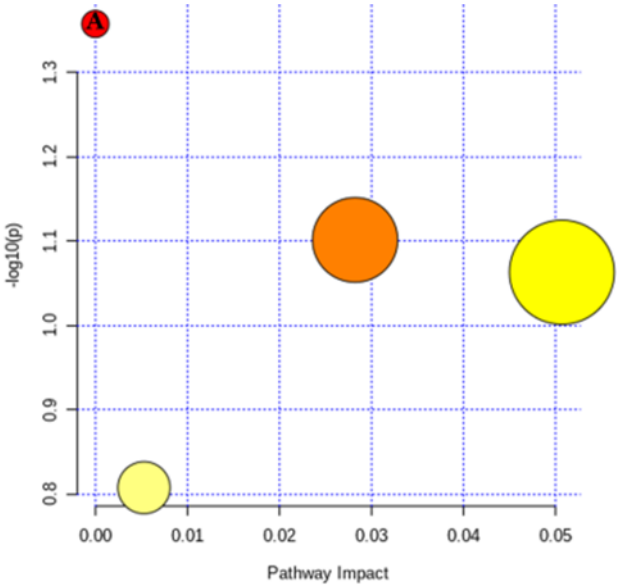

Figure 21 – Metabolic pathways significantly altered in cells exposed to 7.5×10^{-4} nM of 60 nm AuNPs for 24 h. A- Propanoate metabolism (2-hydroxybutyric acid, p=0.043887).

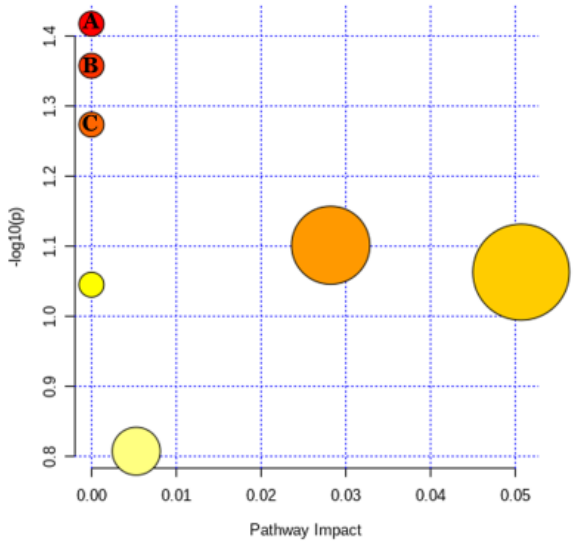

Figure 22 – Metabolic pathways significantly altered in cells exposed to 0.017 nM of AuNSs for 24 h. A- Selenocompound metabolism (L-alanine, p=0.038237); B- Propanoate metabolism (2-hydroxybutyric acid, p=0.043887); C- Alanine, aspartate and glutamate metabolism (L-alanine, p=0.053254).

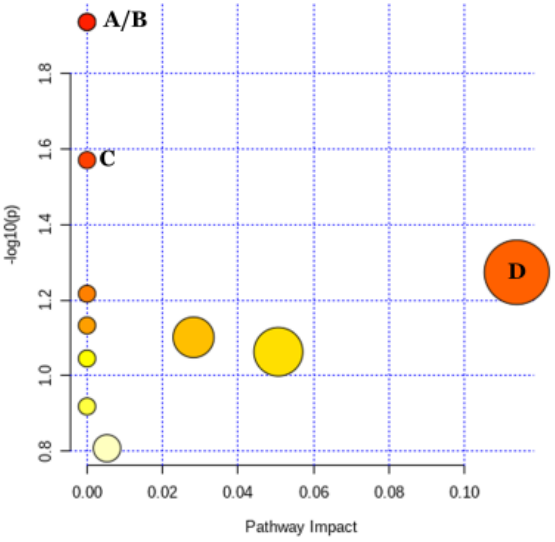

Figure 23 – Metabolic pathways significantly altered in cells exposed to 0.010 nM of AgNSs for 24 h. A- D-Glutamine and D-glutamate metabolism (L-glutamine, p= 0.011575); B- Nitrogen metabolism (L-glutamine, p=0.011575); C- Arginine biosynthesis (L-glutamine, p=0.02687); D- Alanine, aspartate and glutamate metabolism (L-glutamine, p=0.053254).

For the cells exposed to 12, 40, and 60 nm AuNPs, propanoate metabolism (2-hydroxybutyric acid, p=0.043887, 2-hydroxybutyric acid, p=0.029467, and 2-hydroxybutyric acid, p=0.043887, respectively) was altered. In the AuNSs, the selenocompound metabolism (L-alanine, p=0.038237) and alanine, aspartate, and glutamate metabolism (L-alanine, p=0.053254) and propanoate metabolism (2-hydroxybutyric acid, p=0.043887) were dysregulated. The SeNPs altered the aminoacyl-tRNA biosynthesis (L-aspartic acid, L-serine, p=0.002763), arginine biosynthesis (L-aspartic acid, p= 0.02687), nicotinate and nicotinamide metabolism (L-aspartic acid, p=

0.028771), histidine metabolism (L-aspartic acid, p= 0.030669), pantothenate and coenzyme A (CoA) biosynthesis (L-aspartic acid, p= 0.036348), beta-alanine metabolism (L-aspartic acid, p= 0.040123), sphingolipid metabolism (L-serine, p= 0.040123), galactose metabolism (D-galactose, p= 0.051386) and alanine, aspartate and glutamate metabolism (L-aspartic acid, p= 0.053254). Lastly, the AgNSs led to effects in D-glutamine and D-glutamate metabolism (L-glutamine, p= 0.011575), nitrogen metabolism (L-glutamine, p=0.011575), arginine biosynthesis (L-glutamine, p=0.02687) and alanine, aspartate and glutamate metabolism (L-glutamine, p=0.053254).

5. DISCUSSION

As previously mentioned, NMs have great potential for application in several different fields, many of which are related to human exposure, like medicine and food (Khan *et al.*, 2018, Su *et al.*, 2018). Therefore, it is of the utmost importance that their safety is assessed. One of the major organs where NMs are accumulated and can have higher effects is the liver, and, consequently, it is vital to understand the hepatotoxicity of NMs. For this, several models can be used (Zhang *et al.*, 2016). Immortalized liver cell lines have several disadvantages, namely not having the phenotypic characteristics of liver tissue and variance in genes that express enzymes related to metabolism (phase I and II) (Gokduman *et al.*, 2018). Thus, other *in vitro* models are needed to have a more accurate sense of hepatotoxicity, as is the case of primary rat hepatocytes that were used in this study. They retain their functionality for up to 72 h after isolation and allow the study of alterations on the metabolism, induction/inhibition of enzymes, and inter-individual differences, although there can also be inter-species differences, which is a disadvantage (Soldatow *et al.*, 2013).

The characterization of the NPs we obtained was performed through several methods. However, due to either cost or time constraints, not all NPs were analyzed with all the methods. Of the results obtained, we can conclude that the suspensions were stable, since, generally, when the zeta potential is ± 30 mV the NPs solutions are highly stable, and all our NPs (except 40 and 60 nm AuNPs, for which we had no data) had zeta potentials inferior to -30 mV (Bhattacharjee, 2016). With the different techniques, we also obtained different size measurements, which is standard since they are based on distinct principles, and some measure the hydrodynamic size (DLS and NTA), which encompasses the capping as well, and another measure the core diameter (TEM).

None of the AuNPs presented toxicity at the concentrations tested. A study by Fraga et al. (2013) evaluated the viability of HepG2 cells exposed to concentrations from 0-200 μM of 20 nm AuNPs for 24, 48, and 72 h and they concluded that no concentrations caused significative toxicity (Fraga *et al.*, 2013). This agrees with the results we obtained with the 12 and 40 nm, which also resulted in no cytotoxicity at low concentrations. Another study used HepG2 cells and normal human hepatocyte L-02 cell line to assess the cytotoxicity of 5, 20, and 50 nm AuNPs with concentrations from 1.67-12.5 μg/mL for 72 h. No alteration in cell viability was obtained for any concentration of the 20 and 50 nm AuNPs in either cell line, but it was observed with the 5 nm for all concentrations in L-02 cells and the highest concentration in HepG2 cells (Xia *et al.*, 2019). Both studies combined show that smaller AuNPs have higher toxicity but also show that for that to happen, the concentrations needed must be higher than the ones used in our study, explaining why none of the differently sized AuNPs showed any cytotoxicity. We also observed an increase in MTT reduction induced by

the 60 nm AuNPs. It is reasonable to assume, since AuNPs distribute to the mitochondria (Karataş *et al.*, 2009) and since the MTT assay gives mainly, but not exclusively, the metabolic activity in the mitochondria (Stepanenko and Dmitrenko, 2015), that the 60 nm AuNPs could have either potentiated the cellular reduction of MTT or even reduce the MTT themselves, which would explain the increase that we detected. Another reason for this might be interferences of the NPs with the spectrophotometric analysis at the wavelength used for the MTT analysis since this increase in cell viability was not present in the NR test. Interference of NPs with cytotoxic assays have been reported, which is why it is important to use more than one test when studying the cytotoxicity of NPs (Kong *et al.*, 2011). The AuNSs also did not alter cell viability under the assay conditions. Toxicity has been shown for MUA-capped AuNSs of similar size in non-hepatic cells, but only at concentrations much higher than the one used in our study (1-60 μM) (Enea *et al.*, 2019b).

The AgNSs used did not show any toxicity at the concentration tested (0.010 nM). A study was conducted where it was assessed the toxicity and intracellular distribution of 20 nm and 200 nm spherical AgNPs in HepG2 cells exposed to 10, 50, and 100 μg/mL of each NP for 24, 48, and 72 h. An MTT assay was performed and it only showed toxicity after 72 h of exposure to the 200 nm AgNPs at the two higher concentrations, when compared to the 20 nm AgNPs that induced toxicity at the same concentrations already at 24 h (Lankoff *et al.*, 2012). Despite the differences in shape and concentrations of the silver NPs used in this experiment with ours, this study clearly shows that there is no toxicity for low concentrations of larger AgNPs, which validates the results that we obtained since the AgNSs had a concentration of only 0.010 nM.

In this study, we demonstrated that SeNPs even at low concentrations, in the range of nM, cause toxicity to hepatocytes. A study has shown toxicity of SeNPs to buffalo rat liver cells, but only at concentrations of 24 μM and higher, with no toxicity at concentrations from 0.1 to 12 μM (Wang *et al.*, 2020). These are much higher than the concentrations we tested, where the highest one that caused no visible toxicity was 1.67×10^{-3} nM. This could be related to either the size or coating of our SeNPs, since the ones used in the study of Wang et al. (2020) were 78.99 nm and uncoated, while ours have a size of 300 nm and are coated with glucose. Their SeNPs also have a positive zeta potential, while ours has a negative one. This could impact cell uptake and, consequently, the observed toxicity.

Regarding metabolomics, SeNPs elicited the highest number of affected pathways. D-galactose was shown to be increased, and this sugar is usually metabolized into glucose that is then used to produce energy. The accumulation of D-galactose can be a sign of decreased hepatocyte metabolic functions and decreased energy metabolism caused by SeNPs (Coelho *et al.*, 2015). It can also be related to the coating of our SeNPs, since galactose can be synthesized using glucose. In contrast, the nonessential amino acids L-serine and L-

aspartic acid were downregulated, demonstrating that SeNPs can interfere with amino acid biosynthesis. These amino acids take part in many biological pathways, which some were identified to be significantly altered, primarily the metabolism and synthesis of other amino acids, like arginine, histidine, alanine, and glutamate, mainly associated with L-aspartic acid, which will ultimately affect protein metabolism. Another indicator of protein metabolism alteration due to SeNPs exposure is the dysregulation of aminoacyl-tRNA biosynthesis since this is a component of ribosome-dependent protein and peptidoglycan synthesis and protein degradation (Moutiez *et al.*, 2017). Alterations in sphingolipid metabolism due to L-serine downregulation was also evident, which have been proved to play a role not only in the structure of the cell but also to affect several processes, like cell differentiation, growth, and apoptosis (Pralhada Rao *et al.*, 2013). Further dysregulation in energy metabolism was also shown since the pathways of nicotinate and nicotinamide (precursors of NAD^+) metabolism and coenzyme A synthesis (from pantothenate, also known as vitamin B5) were altered, and both NAD^+ and coenzyme A are vital for ATP synthesis in the tricarboxylic acid cycle (TCA cycle) (Yang and Sauve, 2016, Gout, 2018).

There are very few metabolomics studies for the safety assessment of SeNPs. In one study, HepG2 cells were exposed to 16 μM of 100 nm SeNPs for 24 h, after which a targeted metabolomic approach was used to identify altered metabolites (Liu *et al.*, 2020). The principal pathway found dysregulated was protein digestion and absorption, which is in line with our results that indicate that protein metabolism is one of the major metabolic routes affected by SeNPs. Less evident interactions were also seen in sphingolipid and galactose metabolism, as well as aminoacyl-tRNA biosynthesis (Liu *et al.*, 2020), which were also altered in our results. Another study tested the alteration of metabolite excretion in urine after *in vivo* oral exposure of rats to 0.05 or 0.5 mg Se/kg body weight/day of 19 nm SeNPs for 14 days. The results pointed to alteration in protein and fatty acid metabolism (Hadrup *et al.*, 2016), which is, again, relatable to what we uncovered.

When looking at the AgNSs exposed hepatocytes, the pathways that were dysregulated were associated with the alteration of L-glutamine levels. Arginine biosynthesis was altered since it requires L-glutamine, and the metabolism of glutamate, alanine, and aspartate will also be affected, leading to alterations in protein metabolism. The biosynthesis of nucleic acids can also be modified due to interferences in D-glutamate metabolism (Yelamanchi *et al.*, 2016). Glutamine supplies nitrogen, whose metabolism is involved in processes related to purine/pyrimidine nucleotide, nonessential amino acid, and glucosamine-6-phosphate synthesis (Kodama *et al.*, 2020), and its downregulation indicates that AgNSs can potentially cause cell cycle arrest. Another metabolite that was also downregulated was aminomalonic acid, which is a dicarboxylic acid that is synthesized from cysteine by the β-elimination of the sulfur residue, which is a marker of oxidative stress

since cysteine instead of being degraded is potentially being used for GSH synthesis (Ibarra *et al.*, 2014). Decreased levels of cholesterol were also observed, which hints at interference with lipid metabolism since hepatocytes have a role in *de novo* synthesis and metabolism of cholesterol (Zhou and Liu, 2014).

As far as we know, there are no studies of metabolomics made with AgNSs so we will be comparing our results to spherical silver NPs. Mice were intravenously exposed to 8 mg/kg body weight of 26 nm AgNPs and an NMR metabolomics study was performed (Jarak *et al.*, 2017). In the liver, the preliminary results after 6 h of injection showed increased levels of total lipids and cholesterol, which would point to increased lipid synthesis, contrary to the results we observed. However, after 24 and 48 h, the effects were reversed and cholesterol and other lipids decreased, indicating that lipolysis occurs in the liver after a longer period (Jarak *et al.*, 2017), and aligning with the results we obtained with a 24 h exposure. Differences can also be because our study was done *in vitro* while this one was performed *in vivo*, which will inherently have discrepancies. Another *in vivo* study, with rats, was conducted to study the effects of 20 nm citrate capped AgNPs on the metabolome at concentrations of 40 mg/kg/d administered through oral gavage for 4 weeks. Despite none of the altered pathways observed relate to what we observed in our results, the alanine levels were downregulated, impairing urea synthesis and causing liver damage, which can be similar to the outcome of alanine metabolism dysregulation in our results (Xie *et al.*, 2018).

All gold nanoparticles tested in our study produced a decrease in 2-hydroxybutyric acid and consequent dysregulation of propanoate metabolism. Propanoate, or propanoic acid, is a short-chain fatty acid that participates in fatty acid metabolism, so this dysregulation in its metabolism is an indication that gold nanoparticles can interfere with fatty acid metabolism (Fluegge, 2017). This pathway is also related to the catabolism of several amino acids (isoleucine, threonine, valine, and methionine) and cholesterol, with the formation of products that feed into the TCA cycle, implying some sort of effect of gold NPs in energy and protein metabolism (Wongkittichote *et al.*, 2019).

For the smaller AuNPs (12 and 40 nm) a common decreased in L-threonic acid was found. This sugar acid is a metabolite that results from the ascorbic acid oxidative degradation, an important antioxidative pathway, since ROS catalyze these reactions and are, therefore, quenched, impeding their potential oxidative damage (Dewhirst and Fry, 2018). Since L-threonic acid is downregulated, this can mean a decreased ascorbic acid catabolism and the consequent increase of ROS. Another common trait between these AuNPs was the decrease of levels of sugars, namely D-glucopyranose and L-(-)-sorbofuranose, possibly alluding to interference in energy and carbohydrate metabolism. The 12 nm AuNPs evidenced, besides what was already exposed, a decrease in

docosahexaenoic acid. This is a highly unsaturated omega-3 fatty acid that is usually synthesized in the liver from the metabolism of α-linolenic acid, and its decrease can be associated with deficient fatty acid metabolism, consistent with the altered propanoate metabolism mentioned above, and can possibly lead to cognitive or cell/tissue physiology/function problems (Calder, 2016).

For the 60 nm AuNPs, metabolites associated with alterations in fatty acid metabolism disturbances were found dysregulated. Levels of 2-palmitoylglycerol were decreased. As a type of monoacylglycerol, this compound is a product of lipolysis and can be used either for resynthesis of triacylglycerols or metabolism of endocannabinoids, which regulate, among others, lipid metabolism and inflammation (Zhang *et al.*, 2018b). This coupled with the decrease of cholesterol, which was also evident in the AuNSs, further emphasizes the impact of gold nanoparticles in lipid metabolism. The aminomalonic acid levels were decreased, which could indicate oxidative stress caused by these AuNPs.

For the AuNSs some metabolites were noted to be altered in the cells. L-alanine, an amino acid, was up-regulated. A pathway that was found significantly altered that is also related to L-alanine was the selenocompound metabolism, as L-alanine is a metabolite of selenocysteine degradation (Seale *et al.*, 2019). This is an amino acid present in selenoproteins that regulate several cellular processes, like selenium homeostasis and protection against oxidative damage (Schmidt and Simonović, 2012). The increase of L-alanine can mean an upregulation of selenocysteine catabolism, which could lead to dysregulation in protein metabolism and increased oxidative stress. The dysregulation of the alanine, aspartate, and glutamate metabolism also supports the protein metabolism interference of AuNSs.

A study on human colorectal adenocarcinoma cells tested 5 and 30 nm AuNPs at concentrations of 300 μM to analyze the effect of AuNPs size on the metabolism of the cells (Gioria *et al.*, 2016). Propionylcarnitine, a metabolite of the propanoate metabolism, was dysregulated, which corroborates the effect of AuNPs on this pathway, although the levels of propionylcarnitine in this study were increased while the levels of the metabolite we found (2-hydroxybutyric acid) were decreased (Gioria *et al.*, 2016). Propionylcarnitine and other metabolites they found altered (like glycine) can also be related to alterations in carbohydrate metabolism, also noted with our smaller AuNPs (12 and 40 nm), which have a similar size. Differences in results could also be due to the concentration tested, which was significantly higher (300 μM) than the ones used in our study (1.5 and 0.017 nM for the 12 and 40 nm AuNPs, respectively) (Gioria *et al.*, 2016). In HepG2 cells, the overall decrease of all metabolite levels that we observed has also been observed in the previously mentioned study by Lindeque et al. (2018), which had concentrations similar to those we used (0.25-0.5 nM). Briefly, they tested the effects of 0.25 nM of PSSNa-AuNPs and PVP-AuNPs and

0.5 of Cit-AuNPs in HepG2 after a 3 h exposure in the exometabolome (through NMR) and the endometabolome, where they did an untargeted (GC-MS) and target (LC-MS) approach. They hypothesized that the overall decrease in metabolite levels could be related to the metabolites binding themselves to the AuNPs, which could have happened in our study as well (Lindeque *et al.*, 2018). Alterations of energy metabolism were also present in an NMR metabolomics study performed with human cervical cancer-derived cells exposed to AuNPs coated with chitosan (112 nm) and ceria (104 nm) at concentrations of 20 μg/mL (Herance *et al.*, 2019). The pathway of alanine, aspartate, and glutamine metabolism was dysregulated, and this produces metabolites that participate in the TCA cycle and also participate in the synthesis of glutathione, interfering with the antioxidant capacity of the cells (Herance *et al.*, 2019).

A study by our group previously described evaluated the metabolomic alteration in the liver after *in vivo* exposure to AuNPs and AuNSs of equal size and coating (40 nm MUA capped). The rats were exposed to 1.33×10^{11} gold NPs/kg of AuNPs and AuNSs intravenously and after 24 h the liver was extracted and submitted to a pretreatment procedure for the extraction of metabolites, with GC-MS being used to study the metabolite alterations. Increased levels of several amino acids, like L-proline and L-threonine, was mainly associated with AuNSs. This is comparable to what we obtained in our *in vitro* model, despite in our study only L-alanine being upregulated, which can be due to the difference in size (40 vs 60 nm of our AuNSs). Interferences in fatty acid metabolism were caused by both NPs (more pronounced for AuNPs) but, contrary to what we obtained, the levels of fatty acids, like docosahexaenoic acid, were increased. This could be related, again to the size, since in our study the decrease was observed only in the smaller 12 nm AuNPs. Alterations in propanoic acid and ascorbic acid metabolism were also recorded, which relate to the alterations we observed in propanoate metabolism and levels of L-threonic acid (Enea et al., 2019a).

Generally, the NPs we tested affected pathways like energy, lipid, and protein metabolism. Oxidative stress was also present for all NPs. A common effect on the propanoate metabolism was observed only for the AuNPs, which can mean that it is a characteristic alteration related to these NPs.

6. CONCLUSION

In conclusion, the use of metabolomics allowed the identification of altered metabolic pathways caused by several NPs in primary hepatocytes. These were obtained at non-cytotoxic concentrations, which shows that metabolomics has higher sensitivity and can detect early alterations that other classical *in vitro* tests would not.

The alteration in the profile of metabolites elicited by SeNPs showed interference in energy and protein metabolism, amino acid synthesis, and alterations in cell processes and structure.

The AgNSs interfered with protein, lipid, and nucleic acid metabolism, and caused alterations that can be indicative of oxidative stress and cell cycle arrest.

Generally, all gold NPs affected fatty acid/lipid, energy, and protein metabolism as well as caused oxidative stress, with a particular shared dysregulation on the propanoate metabolism. Smaller AuNPs (12 and 40 nm) also presented interferences with carbohydrate metabolism. The larger 60 nm AuNPs exhibited potential initiation of inflammation processes in the exposed hepatocytes.

7. FUTURE PERSPECTIVES

The importance and potential of NMs are increasing each day. However, their mechanisms of toxicity must be clarified. Omics constitute a valuable tool to contribute to this clarification. This is especially important since a lot of the times the effects of NMs are very subtle and, yet, very harmful, something that must be known when one of the main goals is to use them on medicine.

The results of the present study generally agree well with the data reported in the literature, though some of the NPs we studied had either none (AgNSs) or very few (SeNPs) studies using metabolomics. It would be interesting to perform the analysis of the exometabolome, to better understand the results we obtained. This was supposed to be carried out but, due to time constraints associated with the global pandemic, it was impossible in the time we had but will be done at a later date since samples of the culture medium were preserved. Also, some *in vitro* classical assays, like oxidative stress assessment or ATP levels determination, could be realized to further validate the results from our metabolomic studies. Of interest would also be to study the effect of the different coatings on the metabolome, as well as sub-toxic concentrations of the NPs, to see if any other metabolic pathways that we did not see were also altered.

8. REFERENCES

Abbasi, E., Milani, M., Fekri Aval, S., Kouhi, M., Akbarzadeh, A., Tayefi Nasrabadi, H., Nikasa, P., Joo, S.W., Hanifehpour, Y., Nejati-Koshki, K. & Samiei, M., 2016. Silver nanoparticles: Synthesis methods, bio-applications and properties. *Crit Rev Microbiol,* 42**,** 173-80.

Adewale, O.B., Davids, H., Cairncross, L. & Roux, S., 2019. Toxicological Behavior of Gold Nanoparticles on Various Models: Influence of Physicochemical Properties and Other Factors. *Int J Toxicol,* 38**,** 357-384.

Aggarwal, P., Hall, J.B., Mcleland, C.B., Dobrovolskaia, M.A. & Mcneil, S.E., 2009. Nanoparticle interaction with plasma proteins as it relates to particle biodistribution, biocompatibility and therapeutic efficacy. *Adv Drug Deliv Rev,* 61**,** 428-37.

Amberg, A., Riefke, B., Schlotterbeck, G., Ross, A., Senn, H., Dieterle, F. & Keck, M., 2017. NMR and MS Methods for Metabolomics. *Methods Mol Biol,* 1641**,** 229-258.

Atluri, R. & Jensen, K.A., 2017. Engineered Nanomaterials: Their Physicochemical Characteristics and How to Measure Them. *Adv Exp Med Biol,* 947**,** 3-23.

Bachhav, R.M. & Deore, S.N., 2015. A Review on Nanomaterials. *International Journal of Science and Research (IJSR),* 4.

Bastús, N.G., Comenge, J. & Puntes, V., 2011. Kinetically Controlled Seeded Growth Synthesis of Citrate-Stabilized Gold Nanoparticles of up to 200 nm: Size Focusing versus Ostwald Ripening. *Langmuir,* 27**,** 11098-11105.

Bayford, R., Rademacher, T., Roitt, I. & Wang, S.X., 2017. Emerging applications of nanotechnology for diagnosis and therapy of disease: a review. *Physiol Meas,* 38**,** R183-r203.

Berben, L., Sereika, S.M. & Engberg, S., 2012. Effect size estimation: methods and examples. *Int J Nurs Stud,* 49**,** 1039-47.

Berry, M.N., Barritt, G.J., Edwards, A.M. & Burdon, R.H., 1991. *Isolated Hepatocytes: Preparation, Properties and Applications: Preparation, Properties and Applications*: Elsevier Science.

Bhattacharjee, S., 2016. DLS and zeta potential - What they are and what they are not? *J Control Release,* 235**,** 337-351.

Bhattacharjee, S. & Brayden, D.J., 2015. Development of nanotoxicology: implications for drug delivery and medical devices. *Nanomedicine (Lond),* 10**,** 2289-305.

Bierkandt, F.S., Leibrock, L., Wagener, S., Laux, P. & Luch, A., 2018. The impact of nanomaterial characteristics on inhalation toxicity. *Toxicol Res (Camb),* 7**,** 321-346.

Boraschi, D., Italiani, P., Palomba, R., Decuzzi, P., Duschl, A., Fadeel, B. & Moghimi, S.M., 2017. Nanoparticles and innate immunity: new perspectives on host defence. *Semin Immunol,* 34**,** 33-51.

Brar, S.K. & Verma, M., 2011. Measurement of nanoparticles by light-scattering techniques. *TrAC Trends in Analytical Chemistry,* 30**,** 4-17.

Buzea, C. & Pacheco, I., 2017. Nanomaterials and their Classification. *In* A.K. Shukla (ed.) *EMR/ESR/EPR Spectroscopy for Characterization of Nanomaterials.* New Delhi: Springer India, 3-45.

Calder, P.C., 2016. Docosahexaenoic Acid. *Ann Nutr Metab,* 69 Suppl 1**,** 7-21.

Cao, G. & Wang, Y., 2011. *Nanostructures and Nanomaterials: Synthesis, Properties, and Applications*: World Scientific.

Caputo, F., De Nicola, M. & Ghibelli, L., 2014. Pharmacological potential of bioactive engineered nanomaterials. *Biochem Pharmacol,* 92**,** 112-30.

Chen, B., Hong, W., Yang, P., Tang, Y., Zhao, Y., Aguilar, Z.P. & Xu, H., 2020. Nano Zinc Oxide Induced Fetal Mice Growth Restriction, Based on Oxide Stress and Endoplasmic Reticulum Stress. *Nanomaterials (Basel),* 10.

Chen, D., Ganesh, S., Wang, W. & Amiji, M., 2017. Plasma protein adsorption and biological identity of systemically administered nanoparticles. *Nanomedicine (Lond),* 12**,** 2113-2135.

Chen, R., Qiao, J., Bai, R., Zhao, Y. & Chen, C., 2018. Intelligent testing strategy and analytical techniques for the safety assessment of nanomaterials. *Anal Bioanal Chem,* 410**,** 6051-6066.

Cheng, S.-H., Li, F.-C., Souris, J.S., Yang, C.-S., Tseng, F.-G., Lee, H.-S., Chen, C.-T., Dong, C.-Y. & Lo, L.-W., 2012. Visualizing Dynamics of Sub-Hepatic Distribution of Nanoparticles Using Intravital Multiphoton Fluorescence Microscopy. *ACS Nano,* 6**,** 4122-4131.

Ciappellano, S.G., Tedesco, E., Venturini, M. & Benetti, F., 2016. In vitro toxicity assessment of oral nanocarriers. *Adv Drug Deliv Rev,* 106**,** 381-401.

Coelho, A.I., Berry, G.T. & Rubio-Gozalbo, M.E., 2015. Galactose metabolism and health. *Curr Opin Clin Nutr Metab Care,* 18**,** 422-7.

Cremonini, E., Zonaro, E., Donini, M., Lampis, S., Boaretti, M., Dusi, S., Melotti, P., Lleo, M.M. & Vallini, G., 2016. Biogenic selenium nanoparticles: characterization, antimicrobial activity and effects on human dendritic cells and fibroblasts. *Microb Biotechnol,* 9**,** 758-771.

De Melo, A., Seragiotto Amadeu, M., Lancellotti, M., Hollanda, L. & Machado, D., 2015. *The role of nanomaterials in cosmetics: National and international legislative aspects*.

Della Ventura, B., Gelzo, M., Battista, E., Alabastri, A., Schirato, A., Castaldo, G., Corso, G., Gentile, F. & Velotta, R., 2019. Biosensor for Point-of-Care Analysis of Immunoglobulins in Urine by Metal Enhanced Fluorescence from Gold Nanoparticles. *ACS Appl Mater Interfaces,* 11**,** 3753-3762.

Dettmer, K. & Hammock, B.D., 2004. Metabolomics - a new exciting field within the "omics" sciences. *Environ Health Perspect,* 112**,** A396-7.

Dewhirst, R.A. & Fry, S.C., 2018. The oxidation of dehydroascorbic acid and 2,3-diketogulonate by distinct reactive oxygen species. *Biochemical Journal,* 475**,** 3451-3470.

Dolez, P.I., 2015. Chapter 1.1 - Nanomaterials Definitions, Classifications, and Applications. *In* P.I. Dolez (ed.) *Nanoengineering*. Amsterdam: Elsevier, 3-40.

Du, J., Tang, J., Xu, S., Ge, J., Dong, Y., Li, H. & Jin, M., 2018. A review on silver nanoparticles-induced ecotoxicity and the underlying toxicity mechanisms. *Regul Toxicol Pharmacol,* 98**,** 231-239.

Dunn, W.B., Broadhurst, D.I., Atherton, H.J., Goodacre, R. & Griffin, J.L., 2011. Systems level studies of mammalian metabolomes: the roles of mass spectrometry and nuclear magnetic resonance spectroscopy. *Chem Soc Rev,* 40**,** 387-426.

Dunn, W.B. & Ellis, D.I., 2005. Metabolomics: Current analytical platforms and methodologies. *TrAC Trends in Analytical Chemistry,* 24**,** 285-294.

Dusinska, M., Boland, S., Saunders, M., Juillerat-Jeanneret, L., Tran, L., Pojana, G., Marcomini, A., Volkovova, K., Tulinska, J., Knudsen, L.E., Gombau, L., Whelan, M., Collins, A.R., Marano, F., Housiadas, C., Bilanicova, D., Halamoda Kenzaoui, B., Correia Carreira, S., Magdolenova, Z., Fjellsbo, L.M., Huk, A., Handy, R., Walker, L., Barancokova, M., Bartonova, A., Burello, E., Castell, J., Cowie, H., Drlickova, M., Guadagnini, R., Harris, G., Harju, M., Heimstad, E.S., Hurbankova, M., Kazimirova, A., Kovacikova, Z., Kuricova, M., Liskova, A., Milcamps, A., Neubauerova, E., Palosaari, T., Papazafiri, P., Pilou, M., Poulsen, M.S., Ross, B., Runden-Pran, E., Sebekova, K., Staruchova, M., Vallotto, D. & Worth, A., 2015. Towards an alternative testing strategy for nanomaterials used in nanomedicine: lessons from NanoTEST. *Nanotoxicology,* 9 Suppl 1**,** 118-32.

Dusinska, M., Tulinska, J., El Yamani, N., Kuricova, M., Liskova, A., Rollerova, E., Runden-Pran, E. & Smolkova, B., 2017. Immunotoxicity, genotoxicity and epigenetic toxicity of nanomaterials: New strategies for toxicity testing? *Food Chem Toxicol,* 109**,** 797-811.

Egerton, R., 2005. *Physical principles of electron microscopy: An introduction to TEM, SEM, and AEM*.

Elahi, N., Kamali, M. & Baghersad, M.H., 2018. Recent biomedical applications of gold nanoparticles: A review. *Talanta,* 184**,** 537-556.

Enea, M., Araújo, A.M., Almeida, M.P.D., Soares, M.E., Gonçalves-Monteiro, S., Pinho, P.G.D., Pereira, E., Bastos, M.D.L. & Carmo, H., 2019a. A Metabolomic Approach for the In Vivo Study of Gold Nanospheres and Nanostars after a Single-Dose Intravenous Administration to Wistar Rats. *Nanomaterials (Basel, Switzerland),* 9**,** 1606.

Enea, M., Peixoto De Almeida, M., Eaton, P., Dias Da Silva, D., Pereira, E., Soares, M.E., Bastos, M.D.L. & Carmo, H., 2019b. A multiparametric study of gold nanoparticles cytotoxicity, internalization and permeability using an in vitro model of blood–brain barrier. Influence of size, shape and capping agent. *Nanotoxicology,* 13**,** 990-1004.

Fadeel, B., Feliu, N., Vogt, C., Abdelmonem, A.M. & Parak, W.J., 2013. Bridge over troubled waters: understanding the synthetic and biological identities of engineered nanomaterials. *Wiley Interdiscip Rev Nanomed Nanobiotechnol,* 5**,** 111-29.

Favi, P.M., Gao, M., Johana Sepúlveda Arango, L., Ospina, S.P., Morales, M., Pavon, J.J. & Webster, T.J., 2015. Shape and surface effects on the cytotoxicity of nanoparticles: Gold nanospheres versus gold nanostars. *J Biomed Mater Res A,* 103**,** 3449-62.

Filipe, V., Hawe, A. & Jiskoot, W., 2010. Critical evaluation of Nanoparticle Tracking Analysis (NTA) by NanoSight for the measurement of nanoparticles and protein aggregates. *Pharm Res,* 27**,** 796-810.

Fluegge, K., 2017. Propionic acid metabolism, ASD, and vitamin B12: Is there a role for environmental nitrous oxide? *International journal of developmental neuroscience : the official journal of the International Society for Developmental Neuroscience,* 57**,** 21-23.

Fraga, S., Faria, H., Soares, M.E., Duarte, J.A., Soares, L., Pereira, E., Costa-Pereira, C., Teixeira, J.P., De Lourdes Bastos, M. & Carmo, H., 2013. Influence of the surface coating on the cytotoxicity, genotoxicity and uptake of gold nanoparticles in human HepG2 cells. *J Appl Toxicol,* 33**,** 1111-9.

Frens, G., 1973. Controlled Nucleation for the Regulation of the Particle Size in Monodisperse Gold Suspensions. *Nature Physical Science,* 241**,** 20-22.

Frohlich, E., 2012. The role of surface charge in cellular uptake and cytotoxicity of medical nanoparticles. *Int J Nanomedicine,* 7**,** 5577-91.

Frohlich, E., 2017. Role of omics techniques in the toxicity testing of nanoparticles. *J Nanobiotechnology,* 15**,** 84.

Garcia-Leis, A., Garcia-Ramos, J.V. & Sanchez-Cortes, S., 2013. Silver Nanostars with High SERS Performance. *The Journal of Physical Chemistry C,* 117**,** 7791-7795.

Gebel, T., Foth, H., Damm, G., Freyberger, A., Kramer, P.J., Lilienblum, W., Rohl, C., Schupp, T., Weiss, C., Wollin, K.M. & Hengstler, J.G., 2014. Manufactured nanomaterials: categorization and approaches to hazard assessment. *Arch Toxicol,* 88**,** 2191-211.

Gioria, S., Lobo Vicente, J., Barboro, P., La Spina, R., Tomasi, G., Urbán, P., Kinsner-Ovaskainen, A., François, R. & Chassaigne, H., 2016. A combined proteomics and metabolomics approach to assess the effects of gold nanoparticles in vitro. *Nanotoxicology,* 10**,** 736-748.

Gokduman, K., Bestepe, F., Li, L., Yarmush, M.L. & Usta, O.B., 2018. Dose-, treatment- and time-dependent toxicity of superparamagnetic iron oxide nanoparticles on primary rat hepatocytes. *Nanomedicine (Lond),* 13**,** 1267-1284.

Goodman, C.M., Mccusker, C.D., Yilmaz, T. & Rotello, V.M., 2004. Toxicity of gold nanoparticles functionalized with cationic and anionic side chains. *Bioconjug Chem,* 15**,** 897-900.

Gout, I., 2018. Coenzyme A, protein CoAlation and redox regulation in mammalian cells. *Biochemical Society transactions,* 46**,** 721-728.

Guan, B., Yan, R., Li, R. & Zhang, X., 2018. Selenium as a pleiotropic agent for medical discovery and drug delivery. *Int J Nanomedicine,* 13**,** 7473-7490.

Hadrup, N. & Lam, H.R., 2014. Oral toxicity of silver ions, silver nanoparticles and colloidal silver - a review. *Regul Toxicol Pharmacol,* 68**,** 1-7.

Hadrup, N., Loeschner, K., Skov, K., Ravn-Haren, G., Larsen, E.H., Mortensen, A., Lam, H.R. & Frandsen, H.L., 2016. Effects of 14-day oral low dose selenium nanoparticles and selenite in rat-as determined by metabolite pattern determination. *PeerJ,* 4**,** e2601.

Haiss, W., Thanh, N.T.K., Aveyard, J. & Fernig, D.G., 2007. Determination of Size and Concentration of Gold Nanoparticles from UV−Vis Spectra. *Analytical Chemistry,* 79**,** 4215-4221.

Herance, J.R., García, H., Gutiérrez-Carcedo, P., Navalón, S., Pineda-Lucena, A. & Palomino-Schätzlein, M., 2019. A translational approach to assess the metabolomic impact of stabilized gold nanoparticles by NMR spectroscopy. *Analyst,* 144**,** 1265-1274.

Hore, P.J., 2015. *Nuclear magnetic resonance* Oxford: Oxford University Press.

Huang, Y., He, L., Liu, W., Fan, C., Zheng, W., Wong, Y.S. & Chen, T., 2013. Selective cellular uptake and induction of apoptosis of cancer-targeted selenium nanoparticles. *Biomaterials,* 34**,** 7106-16.

Hussain, S., Garantziotis, S., Rodrigues-Lima, F., Dupret, J.M., Baeza-Squiban, A. & Boland, S., 2014. Intracellular signal modulation by nanomaterials. *Adv Exp Med Biol,* 811**,** 111-34.

Ibarra, R., Dazard, J.E., Sandlers, Y., Rehman, F., Abbas, R., Kombu, R., Zhang, G.F., Brunengraber, H. & Sanabria, J., 2014. Metabolomic Analysis of Liver Tissue from the VX2 Rabbit Model of Secondary Liver Tumors. *HPB surgery : a world journal of hepatic, pancreatic and biliary surgery,* 2014**,** 310372-310372.

Jarak, I., Carrola, J., Barros, A.S., Gil, A.M., Pereira, M.L., Corvo, M.L. & Duarte, I.F., 2017. From the Cover: Metabolism Modulation in Different Organs by Silver Nanoparticles: An NMR Metabolomics Study of a Mouse Model. *Toxicol Sci,* 159**,** 422-435.

Jin, G., Zhao, X. & Xu, F., 2017. Therapeutic nanomaterials for cancer therapy and tissue regeneration. *Drug Discov Today,* 22**,** 1285-1287.

Johnson, C.H., Ivanisevic, J. & Siuzdak, G., 2016. Metabolomics: beyond biomarkers and towards mechanisms. *Nat Rev Mol Cell Biol,* 17**,** 451-9.

Karataş, O.F., Sezgin, E., Aydin, O. & Culha, M., 2009. Interaction of gold nanoparticles with mitochondria. *Colloids Surf B Biointerfaces,* 71**,** 315-8.

Kell, D.B., Brown, M., Davey, H.M., Dunn, W.B., Spasic, I. & Oliver, S.G., 2005. Metabolic footprinting and systems biology: the medium is the message. *Nat Rev Microbiol,* 3**,** 557-65.

Kermanizadeh, A., Balharry, D., Wallin, H., Loft, S. & Moller, P., 2015a. Nanomaterial translocation--the biokinetics, tissue accumulation, toxicity and fate of materials in secondary organs--a review. *Crit Rev Toxicol,* 45**,** 837-72.

Kermanizadeh, A., Chauche, C., Brown, D.M., Loft, S. & Moller, P., 2015b. The role of intracellular redox imbalance in nanomaterial induced cellular damage and genotoxicity: a review. *Environ Mol Mutagen,* 56**,** 111-24.

Khan, A., Rashid, R., Murtaza, G. & Zahra, A., 2014. Gold nanoparticles: Synthesis and applications in drug delivery. *Tropical Journal of Pharmaceutical Research,* 13**,** 1169-1177.

Khan, A., Wen, Y., Huq, T. & Ni, Y., 2018. Cellulosic Nanomaterials in Food and Nutraceutical Applications: A Review. *J Agric Food Chem,* 66**,** 8-19.

Khurana, A., Tekula, S., Saifi, M.A., Venkatesh, P. & Godugu, C., 2019. Therapeutic applications of selenium nanoparticles. *Biomed Pharmacother,* 111**,** 802-812.

Kim, D.H., Jarvis, R.M., Xu, Y., Oliver, A.W., Allwood, J.W., Hampson, L., Hampson, I.N. & Goodacre, R., 2010. Combining metabolic fingerprinting and footprinting to understand the phenotypic response of HPV16 E6 expressing cervical carcinoma cells exposed to the HIV anti-viral drug lopinavir. *Analyst,* 135**,** 1235-44.

Kim, E.S., Ahn, E.H., Dvir, T. & Kim, D.H., 2014. Emerging nanotechnology approaches in tissue engineering and regenerative medicine. *Int J Nanomedicine,* 9 Suppl 1**,** 1-5.

Kodama, M., Oshikawa, K., Shimizu, H., Yoshioka, S., Takahashi, M., Izumi, Y., Bamba, T., Tateishi, C., Tomonaga, T., Matsumoto, M. & Nakayama, K.I., 2020. A shift in glutamine nitrogen metabolism contributes to the malignant progression of cancer. *Nature Communications,* 11**,** 1320.

Kong, B., Seog, J.H., Graham, L.M. & Lee, S.B., 2011. Experimental considerations on the cytotoxicity of nanoparticles. *Nanomedicine (Lond),* 6**,** 929-41.

Kumar, A. & Dixit, C.K., 2017. 3 - Methods for characterization of nanoparticles. *In* S. Nimesh, R. Chandra & N. Gupta (eds.) *Advances in Nanomedicine for the Delivery of Therapeutic Nucleic Acids*. Woodhead Publishing, 43-58.

Landsiedel, R., Fabian, E., Ma-Hock, L., Van Ravenzwaay, B., Wohlleben, W., Wiench, K. & Oesch, F., 2012. Toxico-/biokinetics of nanomaterials. *Arch Toxicol,* 86**,** 1021-60.

Lankoff, A., Sandberg, W.J., Wegierek-Ciuk, A., Lisowska, H., Refsnes, M., Sartowska, B., Schwarze, P.E., Meczynska-Wielgosz, S., Wojewodzka, M. & Kruszewski, M., 2012. The effect of agglomeration state of silver and titanium dioxide nanoparticles on cellular response of HepG2, A549 and THP-1 cells. *Toxicol Lett,* 208**,** 197-213.

Lee, S.H. & Jun, B.H., 2019. Silver Nanoparticles: Synthesis and Application for Nanomedicine. *Int J Mol Sci,* 20.

Leso, V., Fontana, L. & Iavicoli, I., 2018. Nanomaterial exposure and sterile inflammatory reactions. *Toxicol Appl Pharmacol,* 355**,** 80-92.

Li, M., Al-Jamal, K.T., Kostarelos, K. & Reineke, J., 2010. Physiologically based pharmacokinetic modeling of nanoparticles. *ACS Nano,* 4**,** 6303-17.

Li, M., Zou, P., Tyner, K. & Lee, S., 2017. Physiologically Based Pharmacokinetic (PBPK) Modeling of Pharmaceutical Nanoparticles. *Aaps j,* 19**,** 26-42.

Liang, X., Wang, H., Zhu, Y., Zhang, R., Cogger, V.C., Liu, X., Xu, Z.P., Grice, J.E. & Roberts, M.S., 2016. Short- and Long-Term Tracking of Anionic Ultrasmall Nanoparticles in Kidney. *ACS Nano,* 10**,** 387-95.

Lima, A.R., Araújo, A.M., Pinto, J., Jerónimo, C., Henrique, R., Bastos, M.L., Carvalho, M. & Guedes De Pinho, P., 2018. GC-MS-Based Endometabolome Analysis Differentiates Prostate Cancer from Normal Prostate Cells. *Metabolites,* 8.

Lima, A.R., Pinto, J., Barros-Silva, D., Jerónimo, C., Henrique, R., Bastos, M.L., Carvalho, M. & Guedes Pinho, P., 2020. New findings on urinary prostate cancer metabolome through combined GC-MS and (1)H NMR analytical platforms. *Metabolomics,* 16**,** 70.

Lin, H., Bu, Q., Cen, X. & Zhao, Y.L., 2012. Current methods and research progress in nanomaterials risk assessment. *Curr Drug Metab,* 13**,** 354-63.

Lindeque, J.Z., Matthyser, A., Mason, S., Louw, R. & Taute, C.J.F., 2018. Metabolomics reveals the depletion of intracellular metabolites in HepG2 cells after treatment with gold nanoparticles. *Nanotoxicology,* 12**,** 251-262.

Liu, T., Xu, L., He, L., Zhao, J., Zhang, Z., Chen, Q. & Chen, T., 2020. Selenium nanoparticles regulates selenoprotein to boost cytokine-induced killer cells-based cancer immunotherapy. *Nano Today,* 35**,** 100975.

Longmire, M., Choyke, P.L. & Kobayashi, H., 2008. Clearance properties of nano-sized particles and molecules as imaging agents: considerations and caveats. *Nanomedicine (Lond),* 3**,** 703-17.

Lorscheidt, S. & Lamprecht, A., 2016. Safety assessment of nanoparticles for drug delivery by means of classic in vitro assays and beyond. *Expert Opin Drug Deliv,* 13**,** 1545-1558.

Lungu, I.I., Holban, A.-M. & Grumezescu, A.M., 2019. Chapter 1 - Superiorities of nanoscale materials in drug delivery. *In* A.-M. Holban & A.M. Grumezescu (eds.) *Materials for Biomedical Engineering*. Elsevier, 1-18.

Luque-Michel, E., Imbuluzqueta, E., Sebastian, V. & Blanco-Prieto, M.J., 2017. Clinical advances of nanocarrier-based cancer therapy and diagnostics. *Expert Opin Drug Deliv,* 14**,** 75-92.

Lv, M., Huang, W., Chen, Z., Jiang, H., Chen, J., Tian, Y., Zhang, Z. & Xu, F., 2015. Metabolomics techniques for nanotoxicity investigations. *Bioanalysis,* 7**,** 1527-44.

Maiyo, F. & Singh, M., 2017. Selenium nanoparticles: potential in cancer gene and drug delivery. *Nanomedicine (Lond),* 12**,** 1075-1089.
Marquis, B.J., Love, S.A., Braun, K.L. & Haynes, C.L., 2009. Analytical methods to assess nanoparticle toxicity. *Analyst,* 134**,** 425-39.
Martin, A. & Sarkar, A., 2019. In Vitro Toxicity Testing of Nanomaterials.
Mcsweeney, P., 2016. The safety of nanoparticles in sunscreens: An update for general practice. *Australian Family Physician,* 45**,** 397-399.
Medina-Reyes, E.I., Garcia-Viacobo, D., Carrero-Martinez, F.A. & Chirino, Y.I., 2017. Applications and Risks of Nanomaterials Used in Regenerative Medicine, Delivery Systems, Theranostics, and Therapy. *Crit Rev Ther Drug Carrier Syst,* 34**,** 35-61.
Mehdi, Y., Hornick, J.L., Istasse, L. & Dufrasne, I., 2013. Selenium in the environment, metabolism and involvement in body functions. *Molecules,* 18**,** 3292-311.
Menni, C., Zierer, J., Valdes, A.M. & Spector, T.D., 2017. Mixing omics: combining genetics and metabolomics to study rheumatic diseases. *Nat Rev Rheumatol,* 13**,** 174-181.
Moldeus, P., Hogberg, J. & Orrenius, S., 1978. Isolation and use of liver cells. *Methods Enzymol,* 52**,** 60-71.
Monopoli, M.P., Aberg, C., Salvati, A. & Dawson, K.A., 2012. Biomolecular coronas provide the biological identity of nanosized materials. *Nat Nanotechnol,* 7**,** 779-86.
Moutiez, M., Belin, P. & Gondry, M., 2017. Aminoacyl-tRNA-Utilizing Enzymes in Natural Product Biosynthesis. *Chem Rev,* 117**,** 5578-5618.
Naik, K. & Kowshik, M., 2017. The silver lining: towards the responsible and limited usage of silver. *J Appl Microbiol,* 123**,** 1068-1087.
Neagu, M., Piperigkou, Z., Karamanou, K., Engin, A.B., Docea, A.O., Constantin, C., Negrei, C., Nikitovic, D. & Tsatsakis, A., 2017. Protein bio-corona: critical issue in immune nanotoxicology. *Arch Toxicol,* 91**,** 1031-1048.
Nie, T., Wu, H., Wong, K.-H. & Chen, T., 2016. Facile synthesis of highly uniform selenium nanoparticles using glucose as the reductant and surface decorator to induce cancer cell apoptosis. *Journal of Materials Chemistry B,* 4**,** 2351-2358.
Padmanabhan, J. & Kyriakides, T.R., 2015. Nanomaterials, inflammation, and tissue engineering. *Wiley Interdiscip Rev Nanomed Nanobiotechnol,* 7**,** 355-70.
Panahi, Y., Mohammadhosseini, M., Nejati-Koshki, K., Abadi, A.J., Moafi, H.F., Akbarzadeh, A. & Farshbaf, M., 2017. Preparation, Surface Properties, and Therapeutic Applications of Gold Nanoparticles in Biomedicine. *Drug Res (Stuttg),* 67**,** 77-87.
Pang, Z., Chong, J., Li, S. & Xia, J., 2020. MetaboAnalystR 3.0: Toward an Optimized Workflow for Global Metabolomics. *Metabolites,* 10.
Patra, J.K., Das, G., Fraceto, L.F., Campos, E.V.R., Rodriguez-Torres, M.D.P., Acosta-Torres, L.S., Diaz-Torres, L.A., Grillo, R., Swamy, M.K., Sharma, S., Habtemariam, S. & Shin, H.S., 2018. Nano based drug delivery systems: recent developments and future prospects. *J Nanobiotechnology,* 16**,** 71.
Peixoto De Almeida, M., Quaresma, P., Sousa, S., Couto, C., Gomes, I., Krippahl, L., Franco, R. & Pereira, E., 2018. Measurement of adsorption constants of laccase on gold nanoparticles to evaluate the enhancement in enzyme activity of adsorbed laccase. *Physical Chemistry Chemical Physics,* 20**,** 16761-16769.
Peng, J. & Liang, X., 2019. Progress in research on gold nanoparticles in cancer management. *Medicine (Baltimore),* 98**,** e15311.
Peters, R.J.B., Bouwmeester, H., Gottardo, S., Amenta, V., Arena, M., Brandhoff, P., Marvin, H.J.P., Mech, A., Moniz, F.B., Pesudo, L.Q., Rauscher, H., Schoonjans, R., Undas, A.K., Vettori, M.V., Weigel, S. & Aschberger, K., 2016. Nanomaterials for products and application in agriculture, feed and food. *Trends in Food Science & Technology,* 54**,** 155-164.
Pietroiusti, A., Bergamaschi, E., Campagna, M., Campagnolo, L., De Palma, G., Iavicoli, S., Leso, V., Magrini, A., Miragoli, M., Pedata, P., Palombi, L. & Iavicoli, I., 2017. The unrecognized occupational relevance of the interaction between engineered

nanomaterials and the gastro-intestinal tract: a consensus paper from a multidisciplinary working group. *Part Fibre Toxicol,* 14**,** 47.
Pietroiusti, A., Stockmann-Juvala, H., Lucaroni, F. & Savolainen, K., 2018. Nanomaterial exposure, toxicity, and impact on human health. *Wiley Interdiscip Rev Nanomed Nanobiotechnol*.
Pluskal, T., Castillo, S., Villar-Briones, A. & Oresic, M., 2010. MZmine 2: modular framework for processing, visualizing, and analyzing mass spectrometry-based molecular profile data. *BMC Bioinformatics,* 11**,** 395.
Poelstra, K., Prakash, J. & Beljaars, L., 2012. Drug targeting to the diseased liver. *J Control Release,* 161**,** 188-97.
Pralhada Rao, R., Vaidyanathan, N., Rengasamy, M., Mammen Oommen, A., Somaiya, N. & Jagannath, M.R., 2013. Sphingolipid Metabolic Pathway: An Overview of Major Roles Played in Human Diseases. *Journal of Lipids,* 2013**,** 178910.
Puisney, C., Baeza-Squiban, A. & Boland, S., 2018. Mechanisms of Uptake and Translocation of Nanomaterials in the Lung. *Adv Exp Med Biol,* 1048**,** 21-36.
Puviani, A.C., Ottolenghi, C., Tassinari, B., Pazzi, P. & Morsiani, E., 1998. An update on high-yield hepatocyte isolation methods and on the potential clinical use of isolated liver cells. *Comp Biochem Physiol A Mol Integr Physiol,* 121**,** 99-109.
Quesada-Gonzalez, D. & Merkoci, A., 2018. Nanomaterial-based devices for point-of-care diagnostic applications. *Chem Soc Rev,* 47**,** 4697-4709.
Ramya, S., Shanmugasundaram, T. & Balagurunathan, R., 2015. Biomedical potential of actinobacterially synthesized selenium nanoparticles with special reference to anti-biofilm, anti-oxidant, wound healing, cytotoxic and anti-viral activities. *J Trace Elem Med Biol,* 32**,** 30-9.
Ribbenstedt, A., Ziarrusta, H. & Benskin, J.P., 2018. Development, characterization and comparisons of targeted and non-targeted metabolomics methods. *PLoS One,* 13**,** e0207082.
Rivera Gil, P., Oberdorster, G., Elder, A., Puntes, V. & Parak, W.J., 2010. Correlating physico-chemical with toxicological properties of nanoparticles: the present and the future. *ACS Nano,* 4**,** 5527-31.
Saifi, M.A., Khan, W. & Godugu, C., 2018. Cytotoxicity of Nanomaterials: Using Nanotoxicology to Address the Safety Concerns of Nanoparticles. *Pharm Nanotechnol,* 6**,** 3-16.
Sakamoto, J.H., Van De Ven, A.L., Godin, B., Blanco, E., Serda, R.E., Grattoni, A., Ziemys, A., Bouamrani, A., Hu, T., Ranganathan, S.I., De Rosa, E., Martinez, J.O., Smid, C.A., Buchanan, R.M., Lee, S.Y., Srinivasan, S., Landry, M., Meyn, A., Tasciotti, E., Liu, X., Decuzzi, P. & Ferrari, M., 2010. Enabling individualized therapy through nanotechnology. *Pharmacol Res,* 62**,** 57-89.
Saleh, T.A. & Gupta, V.K., 2016. Chapter 4 - Synthesis, Classification, and Properties of Nanomaterials. *In* T.A. Saleh & V.K. Gupta (eds.) *Nanomaterial and Polymer Membranes*. Elsevier, 83-133.
Schmidt, R.L. & Simonović, M., 2012. Synthesis and decoding of selenocysteine and human health. *Croat Med J,* 53**,** 535-50.
Schnackenberg, L.K., Sun, J. & Beger, R.D., 2012. Metabolomics techniques in nanotoxicology studies. *Methods Mol Biol,* 926**,** 141-56.
Schneider, C.A., Rasband, W.S. & Eliceiri, K.W., 2012. NIH Image to ImageJ: 25 years of image analysis. *Nature Methods,* 9**,** 671-675.
Seale, L.A., Khadka, V.S., Menor, M., Xie, G., Watanabe, L.M., Sasuclark, A., Guirguis, K., Ha, H.Y., Hashimoto, A.C., Peplowska, K., Tiirikainen, M., Jia, W., Berry, M.J. & Deng, Y., 2019. Combined Omics Reveals That Disruption of the Selenocysteine Lyase Gene Affects Amino Acid Pathways in Mice. *Nutrients,* 11.
Selvamani, V., 2019. Chapter 15 - Stability Studies on Nanomaterials Used in Drugs. *In* S.S. Mohapatra, S. Ranjan, N. Dasgupta, R.K. Mishra & S. Thomas (eds.) *Characterization and Biology of Nanomaterials for Drug Delivery*. Elsevier, 425-444.

Shahbazi, M.A. & Santos, H.A., 2013. Improving oral absorption via drug-loaded nanocarriers: absorption mechanisms, intestinal models and rational fabrication. *Curr Drug Metab,* 14**,** 28-56.
Simard, J.C., Vallieres, F., De Liz, R., Lavastre, V. & Girard, D., 2015. Silver nanoparticles induce degradation of the endoplasmic reticulum stress sensor activating transcription factor-6 leading to activation of the NLRP-3 inflammasome. *J Biol Chem,* 290**,** 5926-39.
Smith, M.J., Brown, J.M., Zamboni, W.C. & Walker, N.J., 2014. From immunotoxicity to nanotherapy: the effects of nanomaterials on the immune system. *Toxicol Sci,* 138**,** 249-55.
Soldatow, V.Y., Lecluyse, E.L., Griffith, L.G. & Rusyn, I., 2013. In vitro models for liver toxicity testing. *Toxicol Res (Camb),* 2**,** 23-39.
Souza, L.R.R., Da Silva, V.S., Franchi, L.P. & De Souza, T.a.J., 2018. Toxic and Beneficial Potential of Silver Nanoparticles: The Two Sides of the Same Coin. *Adv Exp Med Biol,* 1048**,** 251-262.
Stepanenko, A.A. & Dmitrenko, V.V., 2015. Pitfalls of the MTT assay: Direct and off-target effects of inhibitors can result in over/underestimation of cell viability. *Gene,* 574**,** 193-203.
Su, H., Wang, Y., Gu, Y., Bowman, L., Zhao, J. & Ding, M., 2018. Potential applications and human biosafety of nanomaterials used in nanomedicine. *J Appl Toxicol,* 38**,** 3-24.
Tang, S. & Zheng, J., 2018. Antibacterial Activity of Silver Nanoparticles: Structural Effects. *Adv Healthc Mater,* 7**,** e1701503.
Valavanidis, A. & Vlachogianni, T., 2016. Engineered nanomaterials for pharmaceutical and biomedical products new trends, benefits and opportunities. *Pharmaceutical Bioprocessing,* 4**,** 13-24.
Vilanova, O., Mittag, J.J., Kelly, P.M., Milani, S., Dawson, K.A., Radler, J.O. & Franzese, G., 2016. Understanding the Kinetics of Protein-Nanoparticle Corona Formation. *ACS Nano,* 10**,** 10842-10850.
Vinayavekhin, N. & Saghatelian, A., 2010. Untargeted metabolomics. *Curr Protoc Mol Biol,* Chapter 30**,** Unit 30.1.1-24.
Wadhwani, S.A., Shedbalkar, U.U., Singh, R. & Chopade, B.A., 2016. Biogenic selenium nanoparticles: current status and future prospects. *Appl Microbiol Biotechnol,* 100**,** 2555-66.
Wang, B., He, X., Zhang, Z., Zhao, Y. & Feng, W., 2013. Metabolism of nanomaterials in vivo: blood circulation and organ clearance. *Acc Chem Res,* 46**,** 761-9.
Wang, H., He, Y., Liu, L., Tao, W., Wang, G., Sun, W., Pei, X., Xiao, Z., Jin, Y. & Wang, M., 2020. Prooxidation and Cytotoxicity of Selenium Nanoparticles at Nonlethal Level in Sprague-Dawley Rats and Buffalo Rat Liver Cells. *Oxidative Medicine and Cellular Longevity,* 2020**,** 7680276.
Wang, H., Thorling, C.A., Liang, X., Bridle, K.R., Grice, J.E., Zhu, Y., Crawford, D.H.G., Xu, Z.P., Liu, X. & Roberts, M.S., 2015. Diagnostic imaging and therapeutic application of nanoparticles targeting the liver. *Journal of Materials Chemistry B,* 3**,** 939-958.
Wang, J.H., Byun, J. & Pennathur, S., 2010. Analytical approaches to metabolomics and applications to systems biology. *Semin Nephrol,* 30**,** 500-11.
Wang, Y. & Tang, M., 2018. *Dysfunction of various organelles provokes multiple cell death after quantum dot exposure*.
Wang, Y., Yu, L., Kong, X. & Sun, L., 2017. Application of nanodiagnostics in point-of-care tests for infectious diseases. *Int J Nanomedicine,* 12**,** 4789-4803.
Warheit, D.B. & Donner, E.M., 2015. How meaningful are risk determinations in the absence of a complete dataset? Making the case for publishing standardized test guideline and 'no effect' studies for evaluating the safety of nanoparticulates versus spurious 'high effect' results from single investigative studies. *Sci Technol Adv Mater,* 16**,** 034603.
Wilhelm, S., J. Tavares, A., Dai, Q., Ohta, S., Audet, J., Dvorak, H. & C. W. Chan, W., 2016. *Analysis of nanoparticle delivery to tumours*.

Wongkittichote, P., Cunningham, G., Summar, M.L., Pumbo, E., Forny, P., Baumgartner, M.R. & Chapman, K.A., 2019. Tricarboxylic acid cycle enzyme activities in a mouse model of methylmalonic aciduria. *Molecular Genetics and Metabolism,* 128**,** 444-451.
Xia, Q., Huang, J., Feng, Q., Chen, X., Liu, X., Li, X., Zhang, T., Xiao, S., Li, H., Zhong, Z. & Xiao, K., 2019. Size- and cell type-dependent cellular uptake, cytotoxicity and in vivo distribution of gold nanoparticles. *Int J Nanomedicine,* 14**,** 6957-6970.
Xia, Y., Xu, T., Wang, C., Li, Y., Lin, Z., Zhao, M. & Zhu, B., 2018. Novel functionalized nanoparticles for tumor-targeting co-delivery of doxorubicin and siRNA to enhance cancer therapy. *Int J Nanomedicine,* 13**,** 143-159.
Xie, J., Dong, W., Liu, R., Wang, Y. & Li, Y., 2018. Research on the hepatotoxicity mechanism of citrate-modified silver nanoparticles based on metabolomics and proteomics. *Nanotoxicology,* 12**,** 18-31.
Yang, Y. & Sauve, A.A., 2016. NAD(+) metabolism: Bioenergetics, signaling and manipulation for therapy. *Biochimica et biophysica acta,* 1864**,** 1787-1800.
Yeh, Y.-C., Creran, B. & Rotello, V.M., 2012. Gold nanoparticles: preparation, properties, and applications in bionanotechnology. *Nanoscale,* 4**,** 1871-1880.
Yelamanchi, S.D., Jayaram, S., Thomas, J.K., Gundimeda, S., Khan, A.A., Singhal, A., Keshava Prasad, T.S., Pandey, A., Somani, B.L. & Gowda, H., 2016. A pathway map of glutamate metabolism. *J Cell Commun Signal,* 10**,** 69-75.
Yu, M. & Zheng, J., 2015. Clearance Pathways and Tumor Targeting of Imaging Nanoparticles. *ACS Nano,* 9**,** 6655-74.
Yuan, D., He, H., Wu, Y., Fan, J. & Cao, Y., 2019. Physiologically Based Pharmacokinetic Modeling of Nanoparticles. *J Pharm Sci,* 108**,** 58-72.
Yuan, H., Khoury, C.G., Hwang, H., Wilson, C.M., Grant, G.A. & Vo-Dinh, T., 2012. Gold nanostars: surfactant-free synthesis, 3D modelling, and two-photon photoluminescence imaging. *Nanotechnology,* 23**,** 075102.
Yuan, Y.G., Zhang, S., Hwang, J.Y. & Kong, I.K., 2018. Silver Nanoparticles Potentiates Cytotoxicity and Apoptotic Potential of Camptothecin in Human Cervical Cancer Cells. *Oxid Med Cell Longev,* 2018**,** 6121328.
Yun, Y., Dong, Z., Tan, Z., Schulz, M.J. & Shanov, V., 2009. Fibroblast cell behavior on chemically functionalized carbon nanomaterials. *Materials Science and Engineering: C,* 29**,** 719-725.
Zabetakis, K., Ghann, W.E., Kumar, S. & Daniel, M.-C., 2012. Effect of high gold salt concentrations on the size and polydispersity of gold nanoparticles prepared by an extended Turkevich–Frens method. *Gold Bulletin,* 45**,** 203-211.
Zhang, J. & Spallholz, J.E., 2011. Toxicity of Selenium Compounds and Nano-Selenium Particles. *General, Applied and Systems Toxicology*.
Zhang, J., Wang, H., Yan, X. & Zhang, L., 2005. Comparison of short-term toxicity between Nano-Se and selenite in mice. *Life Sciences,* 76**,** 1099-1109.
Zhang, T., Gaffrey, M.J., Thrall, B.D. & Qian, W.J., 2018a. Mass spectrometry-based proteomics for system-level characterization of biological responses to engineered nanomaterials. *Anal Bioanal Chem,* 410**,** 6067-6077.
Zhang, Y., Wang, X., Xie, D., Zou, S., Jin, Q. & Wang, X., 2018b. Synthesis and concentration of 2-monoacylglycerols rich in polyunsaturated fatty acids. *Food Chem,* 250**,** 60-66.
Zhang, Y.N., Poon, W., Tavares, A.J., Mcgilvray, I.D. & Chan, W.C.W., 2016. Nanoparticle-liver interactions: Cellular uptake and hepatobiliary elimination. *J Control Release,* 240**,** 332-348.
Zhou, H. & Liu, R., 2014. ER stress and hepatic lipid metabolism. *Frontiers in genetics,* 5**,** 112-112.
Zhu, M., Nie, G., Meng, H., Xia, T., Nel, A. & Zhao, Y., 2013. Physicochemical properties determine nanomaterial cellular uptake, transport, and fate. *Acc Chem Res,* 46**,** 622-31.